Title
PD AND NI THIN-FILM REACTIONS WITH INP: POSSIBILITIES FOR METAL CONTACTS.

Author
Caron, R.P.

Publication Date
1989-04-01

Center for Advanced Materials

CAM

Pd and Ni Thin-Film Reactions with InP: Possibilities for Metal Contacts

R.P. Caron
(Ph.D. Thesis)

April 1989

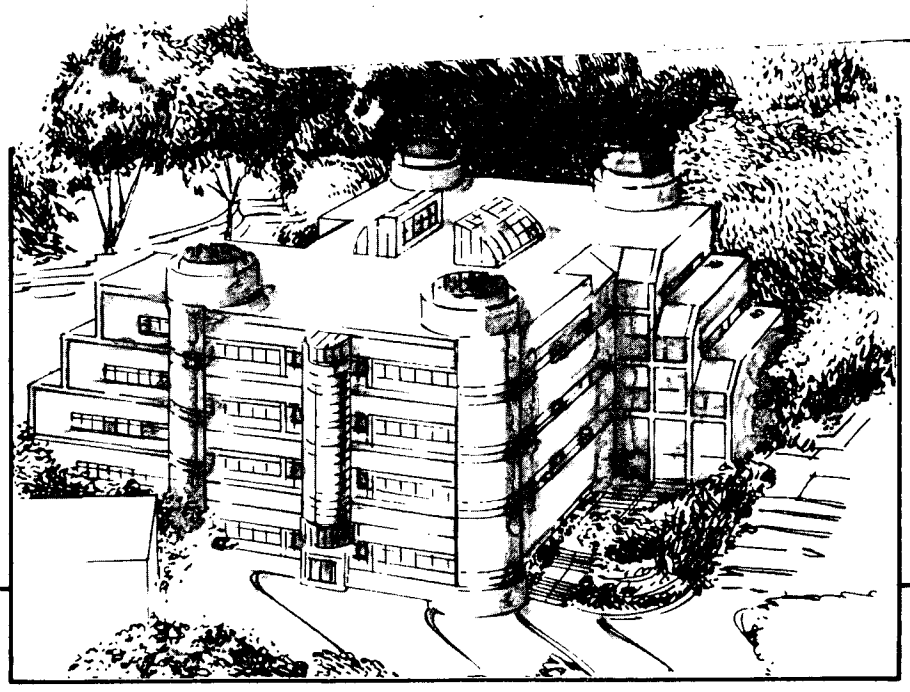

Materials and Chemical Sciences Division

Lawrence Berkeley Laboratory • University of California

ONE CYCLOTRON ROAD, BERKELEY, CA 94720 • (415) 486-4755

Prepared for the U.S. Department of Energy under Contract DE-AC03-76SF00098

DISCLAIMER

Pd AND Ni THIN-FILM REACTIONS WITH InP:

POSSIBILITIES FOR METAL CONTACTS

R'Sue Popowich Caron

Ph.D. Dissertation

April 1989

Department of Materials Science and Mineral Engineering
University of California
Berkeley, CA 94720

and

Center for Advanced Materials
Materials and Chemical Sciences Division
Lawrence Berkeley Laboratory
Berkeley, CA 94720

Pd and Ni Thin-Film Reactions with InP: Possibilities for Metal Contacts

R'Sue Popowich Caron

ABSTRACT

An effort has been made to identify metals whose interactions with InP result in phases with thermal stability, uniform morphology, and good reproducibility. Such metals can be useful as components for ohmic contacts to InP and would be superior to standard Au-Ge contacts, which are known to have very rough morphologies with deep protrusions into the underlying semiconductor. Palladium and nickel were chosen for this study because of good results previously reported for these metals with GaAs.

The Pd/InP reaction began upon deposition. Subsequent annealing at 175°C yielded an amorphous ternary phase, which crystallized into the tetragonal Pd_5InP phase after annealing at 250°C. Both ternary phases contained equal amounts of In and P and had uniform morphologies. Higher temperature anneals (450 to 650°C) yielded globular regions of cubic PdIn interspersed with an amorphous oxide phase. Nevertheless, the low-temperature Pd phases have metallurgical properties that make them desirable as components in contacts for InP devices.

The reaction between Ni and InP can also begin at room temperature with an amorphous ternary phase. Under certain conditions, Ni/InP reaction products at higher temperatures formed layered structures: In-Ni phase/Ni_2P/InP. Subtle changes in the InP native oxide thickness, Ni layer thickness, and annealing ambient gas composition made reproducibility of results unreliable, thereby rendering Ni a less suitable component for InP metallizations.

A effort was made to fabricate a Pd-Ge contact to InP by solid state reaction. Pd was deposited onto the InP substrate and annealed in situ at 180°C to form the amorphous ternary phase. A thicker Ge layer was deposited over this, and the sample was annealed up to 325°C. The reacted layer adjacent to the InP formed a smooth interface and contained the Pd_7P_3 phase, among others. In some regions, Ge was found to grow epitaxially onto the InP substrate. The results suggest that some InP may have regrown onto the substrate during the second heat treatment. Polycrystalline PdGe forms at the Ge/Pd interface upon deposition and grows during subsequent annealing.

ACKNOWLEDGEMENTS

This work would not have been possible without the patient support of my research supervisor, Professor Jack Washburn. I am most especially grateful for the encouragement of Dr. Tim Sands, whom I could count on to see where this work was leading at the times when I couldn't. I would also like to thank Dr. Uli Dahmen for many useful discussions and suggestions throughout the course of this work. I wish to express my appreciation to Dr. Kin Man Yu for his collaboration and for allowing me to include his RBS and glancing-angle x-ray data in this dissertation. I wish to thank Eric Marshall at U.C. San Diego for providing me with the Ge/Pd/InP samples. Discussions with Dr. Kannan Krishnan on amorphous phase formation in the early stages of this work and his help with EDS measurements are gratefully acknowledged.

It has been a pleasure to share an office with Dale Olsen and Jian Ding and to benefit from their insights and support. Dale's expertise in computer analysis of XRD spectra saved me much time by turning raw data into a useful form quickly and accurately. Ding's programs to calculate crystallographic data were invaluable in identifying diffraction patterns from some forty or more possible phases. Many thanks go also to Wendy Swider who kept the TEM specimen preparation lab in good working order and to Don Jurica for his maintenance of the

Philips 400 and his general good humor. I wish also to thank Dr. Carl Lampert for his friendship and occasional financial support.

I would like to thank my parents for their faith in me over the years and, most recently, for the way they have so very enthusiastically taken care of their grandson, Peter, who spent many happy weekends with them while I finished this work. Finally, none of this would have been possible without the unfailing love and support of my husband, David, whose determination in his own work has set a good example for me in mine.

This work was supported by the Strategic Defense Initiative Organization / Innovative Science and Technology administered by the Office of Naval Research under Contract No. N00014-86-K-0668 and by the Director, Office of Energy Research, Office of Basic Energy Sciences, Materials Science Division of the U.S. Department of Energy under Contract No. DE-AC03-76F00098.

TABLE OF CONTENTS

1 INTRODUCTION.....1

1.1 Objective.....1

1.2 Metal Contacts to Semiconductors.....2

1.2.1 Schottky Barrier Contacts.....2

1.2.2 Ohmic Contacts.....4

1.3 Metal/III-V Semiconductor Reactions.....5

1.3.1 GaAs.....5

1.3.2 InP.....7

1.3.3 Contacts Made by Solid-Phase Regrowth Reactions.....8

1.4 Device Requirements.....8

2 EXPERIMENTAL PROCEDURE.....10

2.1 Metal Deposition.....10

2.1.1 Palladium.....10

2.1.2 Nickel.....10

2.1.3 Germanium/Palladium.....11

2.2 Techniques Used.....12

2.3 TEM Specimen Preparation.....14

2.3.1 Plan View.....14

2.3.2 Cross Section.....14

3 Pd/InP SYSTEM.....17

3.1 Experimental Results.....17

3.1.1 Reaction at Room Temperature.....17
3.1.2 Reaction at 175°C.....20
3.1.3 Reaction at 215 and 250°C.....26
3.1.4 Reaction at 450 to 650°C.....30
3.2 Discussion.....34
3.2.1 Low Temperature Phases.....34
3.2.2 High Temperature Phases.....41
3.3 Conclusions.....42

4 **Ni/InP SYSTEM**.....44
4.1 Experimental Results.....44
4.1.1 As-Deposited.....44
4.1.1.1 Deposition 1.....44
4.1.2 Reaction at 240°C.....44
4.1.2.1 Deposition 1.....44
4.1.2.2 Deposition 2.....46
4.1.3 Reaction at 275°C.....47
4.1.3.1 Deposition 1.....47
4.1.3.2 Deposition 2.....50
4.1.4 Reaction at 600°C.....53
4.1.4.1 Deposition 1.....53
4.2 Discussion.....55
4.2.1 Surface Oxide Effect.....57
4.2.2 Metal Thickness Effect.....58
4.2.3 Annealing Ambient Effect.....59
4.3 Conclusions.....61

5 **Ge/Pd/InP METALLIZATION**.....63

5.1 Preliminary Experimental Results.....63

5.1.1 As-Received.....63

5.1.2 Reaction at 205°C.....66

5.1.3 Reaction at 325°C.....68

5.2 Discussion.....77

5.3 Conclusions.....81

6 **CONCLUSIONS**.....82

7 **SUMMARY**.....84

8 **REFERENCES**.....86

Chapter 1

1 INTRODUCTION

1.1 Objective

The metal contact to a semiconductor device provides communication between the device and the external circuit. It is crucial that the contact exhibit good electrical behavior both initially and throughout the lifetime of the device. As devices are made smaller the requirements for metal contacts become more stringent. Metallizations must be thermally stable during processing treatments and morphologically uniform on a scale of tenths of microns.

For III-V semiconductor devices, standard ohmic contacts are based on Au-Ge eutectic materials. The films are heated to the eutectic temperature, thus forming the contact by a liquid phase process. The morphology of these contacts is very rough and irregular with deep protrusions into the underlying semiconductor. Furthermore, the metallurgy of systems with five or more components is quite complicated and not well understood.

Knowing the nature of the interactions in relatively simple metal(M)-In-P ternary systems or M-InP pseudo-binary systems is a good first step toward understanding more complicated metallization schemes. At present, phase formation data on these systems are scarce.

In this investigation an effort has been made to find a

metal whose interactions with InP result in phase(s) with good metallurgical properties; thermal stability and regular, uniform morphology(ies). The metals chosen for this study were Pd and Ni because of good results reported previously[1,2,3] for these metals with GaAs.

1.2 Metal Contacts to Semiconductors

The metal contact to a semiconductor device allows current to flow between the active region of the device and the external circuit. The metallization must have electrical properties that do not conflict with or overshadow the function of the device. Based on current-voltage characteristics there are two distinct types of metal-semiconductor contact: Schottky barrier (rectifying) and ohmic (linear).

1.2.1 Schottky Barrier Contacts

In general, when a metal is deposited onto a semiconductor and the flow of current is measured as a function of voltage rectifying behavior is observed. For forward bias current flows easily, and for reverse bias current flow is negligible. Schottky[4] explained this as due to a potential barrier that arises from charge transfer between metal and semiconductor. The barrier height, ϕ_b, is the difference between the metal work function, ϕ_m, and the semiconductor electron affinity, X_{sc}, i.e., $\phi_b = \phi_m - X_{sc}$. This value for the barrier energy is known as the Schottky limit.

In another classical model, the Bardeen model,[5] the

barrier height is independent of the metal work function. At the surface of a semiconductor crystal the regular periodicity of the lattice is disturbed, giving rise to surface states. These can be either occupied or empty depending on their energy level relative to the Fermi energy (E_F) at the surface. If there are sufficient numbers of surface states at the M/SC interface, ϕ_b is independent of ϕ_m. The Bardeen limit of the barrier energy is given by $\phi_b = E_g - \phi_o$, where ϕ_b is the Schottky barrier energy, E_g is the band gap energy of the semiconductor, and ϕ_o is the neutral energy level to which surface states are filled when the surface is neutral.

For a real M/SC contact the barrier energy lies somewhere between the Schottky and Bardeen limits. For many III-V semiconductors it has been found that the Fermi level is pinned at the same energy independent of the metallization. The classical models are inadequate to explain this observation. Currently, there is a vigorous debate about the mechanism of Schottky barrier formation and the associated Fermi level pinning. A brief description of the main theories follows.

According to the Unified Defect Model (UDM)[6,7,8] energy liberated during metal deposition creates defects in the semiconductor which give rise to surface states. This is based upon the observations that for a particular semiconductor material E_f is pinned at the same level even at submonolayer coverage and regardless of the overlayer atom

(metal, gas, or other semiconductor).

The Effective Work Function Model (EWFM)[9,10] proposes that the Fermi level is related to the work functions of microclusters of one or more interface phases. The sources of these phases are oxygen contamination and metal-semiconductor reactions. A weighted average of the work functions of the various phases yields an effective work function that can be used in the original Schottky model.

Another theory is that Fermi level pinning is determined by inherent properties of ideal metal-semiconductor interfaces. In the Metal Induced Gap States theory (MIGS),[11,12] tails of the metal wave functions extend into the semiconductor causing an exponential decay of metal states beyond the interface. These states determine the pinning of the Fermi level.

Other explanations for Fermi level pinning behavior have included extrinsic defects due to impurity or metal atom migration into the semiconductor crystal[13] and dangling bonds associated with vacancy or antisite defects at or near semiconductor surfaces.[14]

1.2.2 Ohmic Contacts

An ohmic contact allows current to flow into a device with a voltage drop that is insignificant compared to the drop across the active region of the device regardless of the polarity of the applied voltage. The most common type is the tunneling ohmic contact. As the doping in the semiconductor

is increased, the width of the barrier becomes thinner. For sufficiently high doping, quantum-mechanical tunneling of electrons through the barrier can occur. This tunneling leads to ohmic behavior that is strongly dependent on doping concentration.

1.3 Metal/III-V Semiconductor Reactions

1.3.1 GaAs

Reactions between single metal thin-films and GaAs can be grouped into three categories based on the temperatures at which the first reaction occurs. As might be expected, strongly bonded refractory metals such as Nb, Ta, Mo, and W do not react with GaAs until the temperature reaches 500-700°C.[15,16,17,18] The reaction products are M-As compounds and either M-Ga phases or metallic Ga. At temperatures from 250-500°C many near-noble transition metals (e.g. Rh, In, Pt) are able to penetrate the thin native oxide on the GaAs surface and begin reacting with GaAs. These metals are bonded less strongly than refractory metals, allowing them to be mobile at these lower temperatures. Layered binary phases in the sequence M-Ga/M-As/GaAs are formed. Since both the Ga and M can diffuse, the original GaAs native oxide layer is found between the M-Ga and M-As layers.[19] The lowest temperature reactions (< 250°C) occur for the metals, Pd and Ni. Ga and As are less mobile at these temperatures. Metal atom diffusion predominates, resulting in formation of intermediate ternary M_xGaAs phases.[20,21,22,23,24] At higher temperatures where

Ga and As can move also, the ternary phases decompose and react further to form either PdGa and $PdAs_2$ or NiGa and NiAs.

With conventional manufacturing techniques, it is inconvenient and expensive to fabricate contacts under ultra-high vacuum conditions. Consequently, there is always a native oxide on the semiconductor surface. So it is necessary to find metallization schemes that will make good, reproducible contacts in spite of this. A useful feature of Ni and Pd is that they can penetrate very thin native oxides (< 2nm) at temperatures below 80°C. However if the oxide is as thick as 3-5 nm, there is no Ni reaction even at temperatures as high as 220°C.[25] This makes Pd unique and especially useful since it can penetrate even these thicker oxides at temperatures below 80°C.[26]

In practice, metal contacts to GaAs devices are multielemental; the most common ones are based on the Au-Ge eutectic mixture. Although the metallurgy of the standard Au-Ge-Ni ohmic metallization[27] is complex and not well understood, many problems are quite apparent. The film is heated to the eutectic temperature, thus forming the contact by a liquid phase process. This does not lend itself to formation of sharp, flat interfaces, but rather to irregularity on a large scale with poor morphology and deep protrusions into the underlying substrate.[28,29,30] In spite of this, these contacts have yielded acceptable resistivities with reasonable reproducibilities. As devices are scaled down to submicron

dimensions, requirements for metal contacts become more stringent. Small protrusions from the contact into the semiconductor, which were tolerable before, may now reach the active region of the device, thus shorting it out and rendering it inoperable.

A more thorough discussion of GaAs contact metallurgy can be found in the reviews by Sands,[31] Palmstrom and Morgan,[32] and G.Y. Robinson[33].

1.3.2 InP

Most information in the literature about single metal/InP systems is from investigations to find correlations between Schottky barrier height and some property of the metal or interface (see, for example, Hokelek and Robinson[34], Brillson et al.[35], and Kendelewicz et al.[36] and references therein). Many of these studies have concentrated on interactions of very thin or even submonolayer coverages of metal on InP at low temperatures where reaction kinetics are of little importance. Consequently, metastable and intermediate phases, which may be useful in designing metallizations, are unlikely to be seen.

There is so little metallurgical data available on M-InP systems that it is not possible to discuss trends in these reactions as for the M-GaAs systems. One system of interest that has been studied is Ni-InP. This will be discussed in Chapter 4.

1.3.3 Contacts Made by Solid-Phase Regrowth Reactions

A novel, new approach to GaAs contact fabrication, which involves a series of solid-state reactions in a multielemental metallization scheme has been developed by Sands, Marshall, and Wang.[37] They refer to this as solid-phase regrowth of compound semiconductors by reaction-driven decomposition of intermediate phases. A layered arrangement of thin films in the sequence M'/M/AB is deposited onto a compound semiconductor substrate AB. At low temperatures, metal M reacts with AB to form an intermediate ternary phase, M_xAB, and metal M' is relatively inert. A subsequent reaction at higher temperatures between the M' layer and the intermediate phase results in decomposition of M_xAB, epitaxial regrowth of a doped or lightly-alloyed layer of AB, and formation of a M_yM' compound. Since all reactions take place at rather low temperatures and in the solid state, uniform interfaces with regular morphologies are expected. Doping of the regrown AB layer gives an n^+ layer at the interface as required for a tunneling ohmic contact.

Reactions of this type have been shown to occur for Ge/Pd/GaAs,[38] Si/Pd/GaAs,[39] and Si/Ni/GaAs.[40]

1.4 Device Requirements

As devices are made smaller, the requirements for metal contacts become more stringent. For example, smaller contact areas will require metallization systems with lower contact

resistivities. A smooth interface morphology will be needed to minimize short channel effects and high-drain electric fields in III-V transistors. At the same time, techniques for fabricating contacts must be simple enough to be used in manufacturing. Although techniques requiring ultra-high vacuum (such as molecular beam epitaxy) can be useful in making well-characterized materials for laboratory study, they are too costly for most large-scale device production. What are needed are metallization systems whose thermodynamic and kinetic properties allow for easily reproducible reactions under manufacturing conditions.

Chapter 2

2 EXPERIMENTAL PROCEDURE

2.1 Metal Depositions

Sulphur-doped n^+ ($n=5 \times 10^{18}$ cm^{-3}) or nominally undoped InP wafers in [100] orientation were used in this study. Three different depositions were done.

2.1.1 Palladium

For the Pd deposition, the wafer was degreased and then etched in $H_2SO_4:H_2O_2:H_2O$ (5:1:1) for 2 min. It was rinsed in deionized water and blown dry with N_2. Palladium was deposited to a 40-nm thickness by electron beam evaporation in a vacuum of 10^{-6} Torr. Although the substrate temperature was not monitored during this step, it is estimated to have been less than 50°C. The wafer was cut into pieces that were annealed for 30 min in a tube furnace with a flowing forming gas (95% Ar - 5% H_2) atmosphere at temperatures from 175 to 650°C. Additional 60-min heat treatments were done at 175°C. Samples to be annealed at 250°C and higher were capped first on both sides with a 200-nm SiO_2 layer formed by plasma-enhanced chemical vapor deposition (PECVD). It is estimated that the sample temperature did not exceed 200°C during this step.

2.1.2 Nickel

For the Ni depositions, standard cleaning for the InP wafers was as follows. They were degreased in warm

trichlorethylene, rinsed in warm acetone, and then in methanol. They were etched for 2 min in H_2SO_4:H_2O_2:H_2O (5:1:1) and rinsed in deionized water. Later it was suspected that this standard cleaning was inadequate, and for some depositions the wafers underwent an additional step of etching in 10% HF solution for 2 min. They were placed in an evaporation chamber that was then pumped to a pressure of either 1×10^{-6} or 1×10^{-7} torr. Ni was deposited onto the wafers by electron beam evaporation to a thickness of 30, 74, or 100 nm. Residual gold from the evaporation chamber was also present in the films in the amount of 0.3%. The wafers were cut into pieces and annealed at 240 or 275°C for 30 min in either Ar-5%H_2 or N_2-4%H_2. Some pieces annealed at 275°C were covered later with about 210 nm SiO_2 using PECVD and heat treated again in flowing N_2-4%H_2 at 600°C for 1 h.

2.1.3 Germanium - Palladium

Samples for Pd-Ge solid state reaction were made by depositing Pd onto an InP substrate followed by a Ge overlayer. The wafers were cleaned with organic solvents and blown dry with N_2. The wafers were dipped in H_2SO_4 and then etched in H_2SO_4:H_2O_2:H_2O (5:1:1) for 2 min. They were rinsed in water for 2 min and blown dry with N_2. Cleaning for sample 1 ended here. Sample 2 underwent additional steps. It was etched in HCl:HF:H_2O:H_2O_2 (1:1:4:5 drops per 12 ml solution) for 3 min, rinsed in water and blown dry with N_2. Both samples were clipped onto a molybdenum block in an evaporation

chamber that was pumped subsequently to 1.2 x 10^{-8} torr. The Pd was deposited to a thickness of 40 nm by electron beam evaporation at a rate of 0.7 nm/sec in a vacuum of 7 x 10^{-8} torr. The samples were annealed in situ at 180°C for 30 min. They were cooled to 29°C, and 120 nm Ge was deposited at a rate of 1 nm/sec in a vacuum of 2 x 10^{-7} torr. Ex situ annealing at 205 and 325°C was performed in a tube furnace with a flowing forming gas atmosphere.

2.2 Techniques Used

The samples were examined using Auger electron spectroscopy (AES), Rutherford backscattering spectrometry (RBS), x-ray diffraction (XRD), Seeman-Bohlin x-ray diffraction (SBXRD), transmission electron microscopy (TEM), and energy-dispersive x-ray spectroscopy (EDS). Not all techniques were used on every sample. For example, Pd/InP samples were not examined with RBS. The peak energy in an RBS spectrum is related to the atomic weight of the element. Since the weights of Pd and In are very close (106 and 115, respectively), their signals overlap, and the position of one relative to the other near the surface cannot be resolved. Auger depth profiles were obtained with a Perkin Elmer PHI 600 system using a 10 keV primary electron beam and a 2 keV Ar sputtering beam. RBS measurements were made using 2.0 MeV $^{4}He^{+}$ ions from a 2 MeV Van de Graaf accelerator. A silicon surface barrier detector was positioned at a backscattering angle of 170°. The energy resolution of the system was about 18 keV.

The x-ray diffraction was performed on a Siemens Kristalloflex diffractometer using Cu Kα incident radiation. Samples were scanned over a 2θ range from 15° to 100°. Seeman-Bohlin XRD was done at glancing angles to the specimen surface. The 2θ range used was from 22° to 120°. This range measures interplanar spacinge from 0.09 to 0.40 nm. TEM specimens were imaged using a Siemens 102 or a Philips 400 electron microscope operated at 100 kV or a JEOL JEM 200CX operated at 200 kV. Kevex high-angle x-ray detectors (System 8000) mounted on the 400 and the 200CX were used to gather EDS data. Elemental analysis was done using the thin-film approximation, which assumes the sample is thin enough that neither absorption nor fluorescence corrections are needed. Atomic ratios were calculated using the technique of Cliff and Lorimer[41] where for any two elements, A and B, the ratio of their x-ray intensities, I_A/I_B, is directly related to the ratio of their mass concentrations, C_A/C_B. This can be described by:

$$C_A/C_B = k_{AB}\ I_A/I_B.$$

The k-factor (k_{AB}) is independent of sample thickness and composition if both intensities are measured at the same time. In this study, theoretically-derived k-factors were used.

2.3 TEM Specimen Preparation

2.3.1 Plan View

Specimens for TEM were prepared in plan-view by chemical thinning. Metallized InP pieces less than 3 mm in size were cut and ground on the InP side to about 150-μm thickness. The specimen was mounted onto a teflon holder with the metal side down using acid-resistant lacquer. Care was taken that the metal side and edges of the InP side were protected. The exposed InP was placed in contact with a slow stream of chlorine-methanol solution. The specimen was removed at regular intervals (from 2 min to 15 sec) and examined in a light microscope. Chemical-thinning was complete when either a perforation or a round shape with a flat shiny bottom, indicating exposure of the metallized region, was observed. Acetone was used to remove the specimen from the holder and to wash it thoroughly. The specimen was attached to a 3-mm Cu TEM grid with a 1 x 2 mm hole using Devcon Two-Ton Epoxy. Some of these were cooled to liquid nitrogen temperature and thinned further from both sides in a Gatan ion-milling machine operated at 2.5 kV using Ar^+ ions and with a total beam current of 0.5 ma.

2.3.2 Cross Section

Cross-sectional specimens were prepared using the following procedure. With metallized layers facing each other, small pieces (approximately 2 x 3 mm) of the wafers were glued together with epo-tek H20E silver epoxy (from epoxy

technology, inc.) and cured at 90°C for 1 h. The specimen was then ground perpendicular to the joint until it was flat on both sides and the 2-mm thickness was reduced to about 300 μm. One side was polished with succeedingly finer abrasive powders until final polish was achieved with 0.05 μm Al_2O_3 powder. The specimen was mounted, polished side down, onto the holder of a South Bay Technology Model 515 dimpling machine using Crystalbond 509 (manufactured by Aremco Products, Inc.). The thickness of the specimen was reduced to about 50 μm with a large brass grinding wheel (16 mm diameter, 3 mm thickness) and 15 μm SiC grit. Grinding was stopped at regular intervals so that the thickness could be monitored with an optical measuring microscope. The sample was dimpled using a smaller stainless steel wheel (14 mm diameter, 1.5 mm thickness) wrapped with Buehler Microcloth polishing cloth and 1 μm Al_2O_3 powder. Dimpling proceeded until the specimen thickness at the center was about 8 μm. A 14-mm felt wheel and 0.05 μm Al_2O_3 powder were used for the final polish. There was no measurable thickness change during this last step. A Cu TEM grid, 3mm in diameter, with either a 1 x 2 or a 0.4 x 2 mm slot was mounted onto the specimen with Devcon Two-Ton epoxy. This was allowed to set overnight. The next day the specimen, with grid attached, was removed from the sample holder by soaking in acetone. The acetone dissolved the Crystalbond while leaving the epoxy undisturbed. The specimen was washed carefully in acetone several times. Final thinning to

perforation was done from both sides at liquid nitrogen temperature in a Gatan ion-milling machine operated at 2.5 kV with Ar^+ ions at an angle of 11 - 12° and a total beam current of 0.5 ma. Because of the large difference in their atomic weights, the Pd milled at a much slower rate that the InP. This made it difficult to produce thin regions that were continuous across both the Pd-reacted layer(s) and the underlying InP substrate. Dimpling before ion milling and ion-milling at very shallow angles (11 - 12°) helped to alleviate this problem.

Chapter 3

3 Pd/InP SYSTEM

3.1 Experimental Results

3.1.1 Reaction at Room Temperature

Diffusion of Pd into the InP substrate had begun even before annealing, as seen in Fig. 3.1. The AES depth profile shows a 25-30 nm layer of Pd on the surface followed by a diffused region that has slightly decreasing Pd and slightly increasing In and P concentrations with depth. Although ion mixing during sputtering can cause the appearance of interdiffusion, the fact that the slopes of the Pd, In, and P profiles change with time is a clear indication that the sample contains an interdiffused region. There was good agreement between the XRD spectrum and peaks expected for Pd and InP. Plan-view TEM showed a polycrystalline film with a grain size on the order of 10 nm. Most selected area diffraction patterns (SAD) showed polycrystalline Pd rings and the [100] spot pattern from the InP substrate. In some thinner regions where all the InP substrate had been removed, there were also additional rings with amorphous character.

A TEM image of this material viewed in cross section is shown in Fig. 3.2. There is a thick layer of unreacted Pd at the surface. At the Pd/InP interface another layer about 10 nm in thickness can be seen. Contrast from this layer did not change with specimen tilt. Microdiffraction from this region

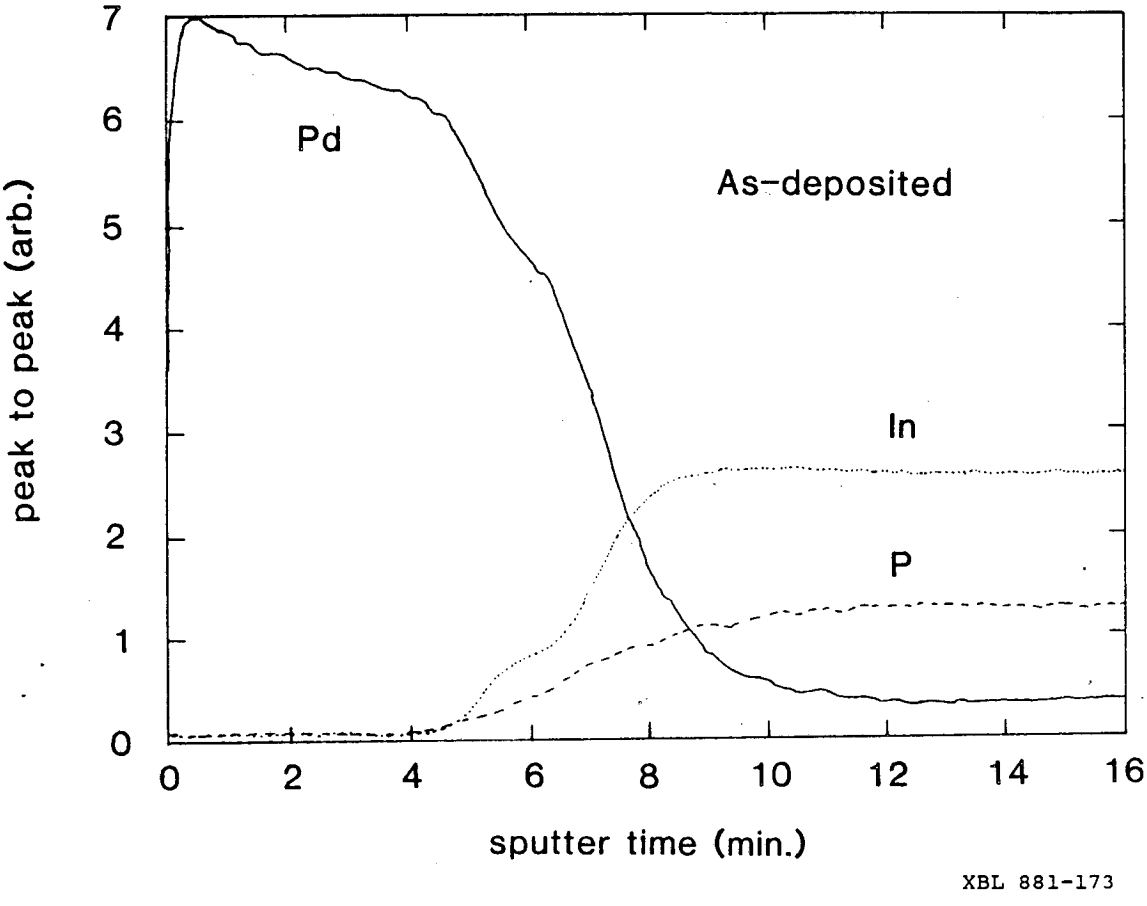

Figure 3.1 AES depth profile of as-deposited Pd/InP sample showing that interaction of metal with substrate has begun.

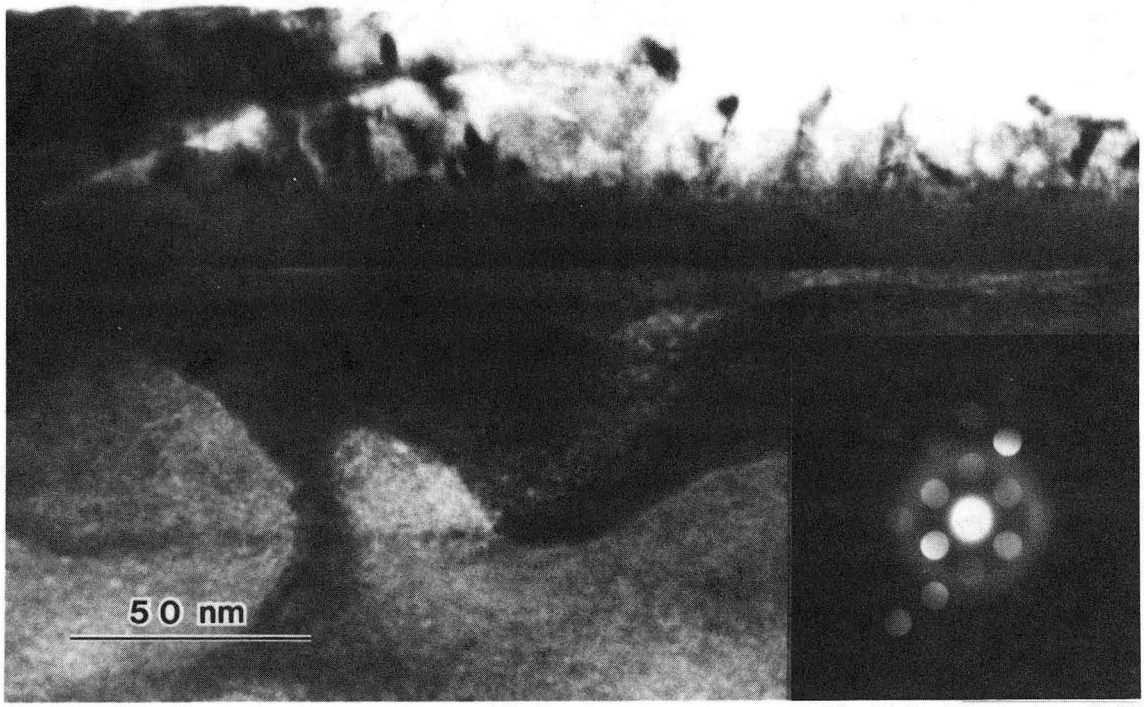

XBB 891-356

Figure 3.2 Cross-sectional TEM image of Pd/InP sample as received. Reaction between the metal and substrate has begun with formation of an amorphous phase.

yielded patterns consistent with an amorphous structure. It should be noted that this material underwent a 100°C 30-min heat treatment during preparation of the cross-section specimen for TEM. This may have accelerated the room temperature reaction.

3.1.2 Reaction at 175°C

For samples annealed at 175°C for one hour, AES data (Fig. 3.3) showed that consumption of the Pd layer was nearly complete. There was a thin layer of either Pd or a Pd-rich ternary compound at the surface. The next layer extended to the InP substrate and was of composition Pd_xInP, with x varying from about 4 near the surface to 3 near the substrate.

Plan-view TEM of a sample annealed at 175°C for 30 min. (Fig. 3.4) shows a continuous film with amorphous character. The diffraction pattern shows diffuse amorphous rings with interatomic distances of about .230 and .127 nm, sharper polycrystalline Pd rings and a few diffuse spots. The edge of the film still in contact with the InP substrate has recrystallized in a continuous band about 1 μm wide with a grain size of about 60-70 nm. These regions yield polycrystalline diffraction patterns with strong texture. The strongest reflections can be indexed as the tetragonal phase Pd_5InP, previously reported by El-Boragy and Schubert[42] as $Pd_{72}In_{14}P_{14}$ with lattice parameters, a=0.3928 nm, c=0.6917 nm.

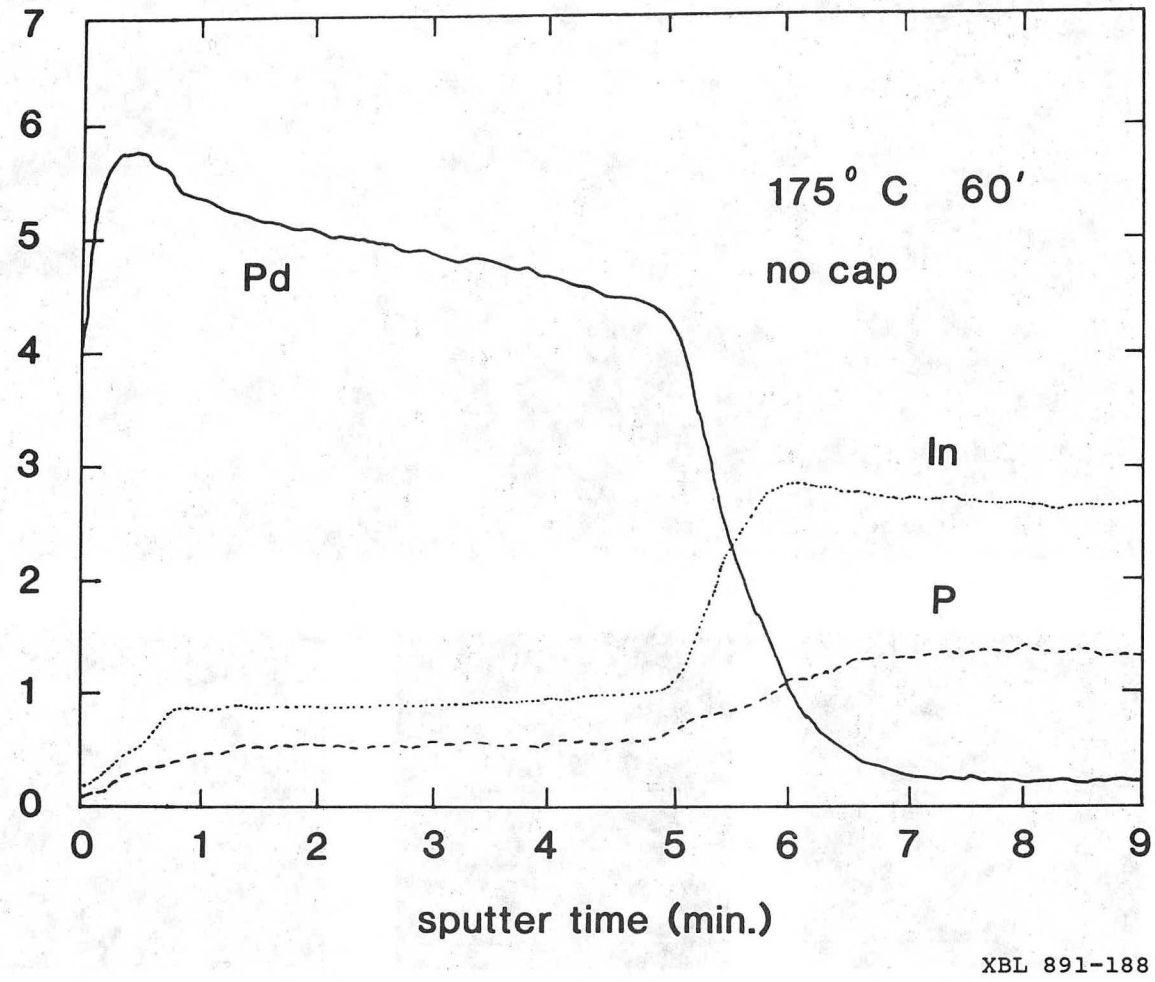

Figure 3.3 AES depth profile of Pd/InP sample annealed at 175°C for 1 hr. Most of the film is a ternary Pd_xInP phase. At the surface, there is a layer less than 5 nm in thickness that is either unreacted Pd or a very Pd-rich region of the ternary phase.

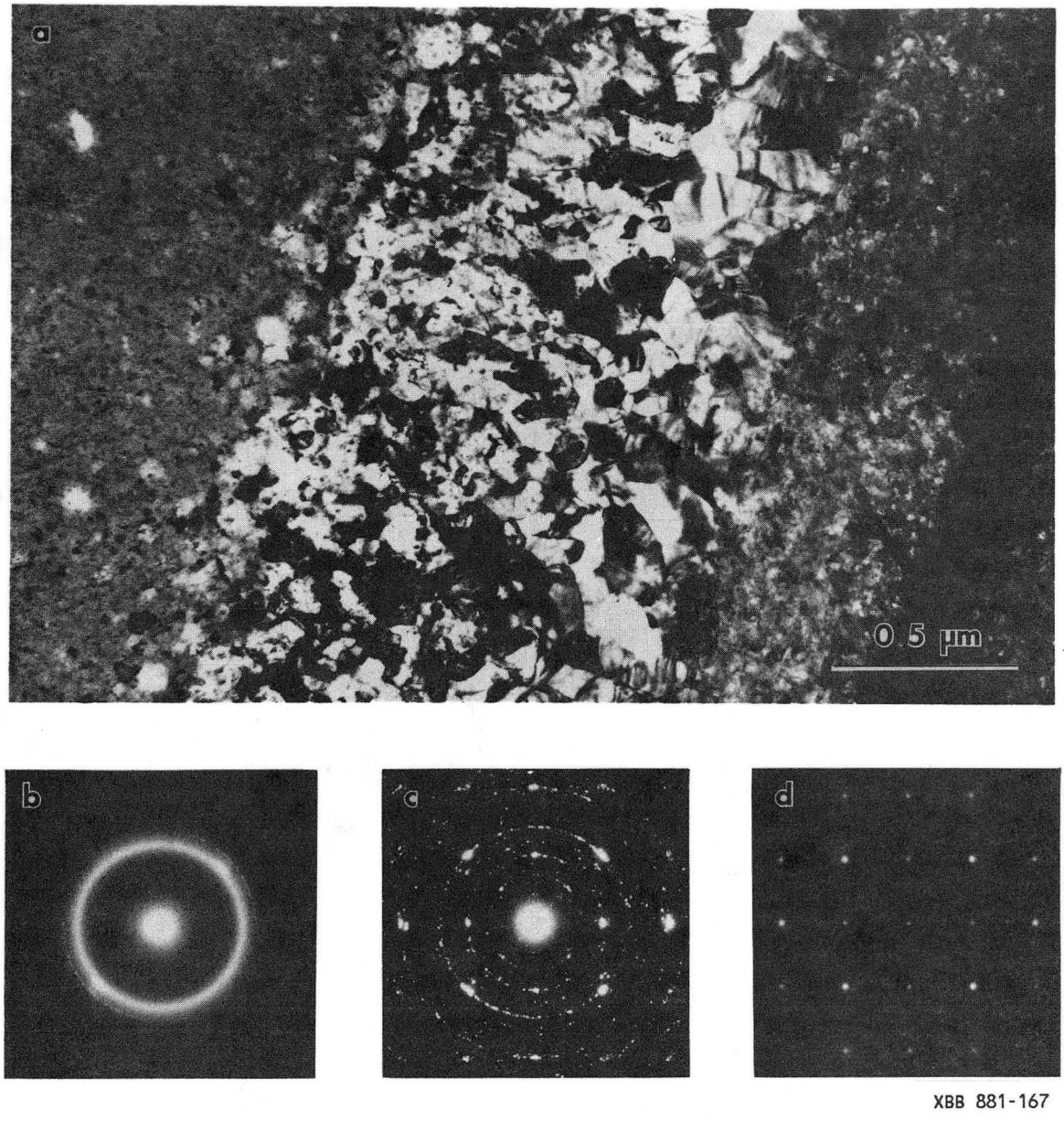

Figure 3.4 (a) Plan-view TEM micrograph of a Pd/InP sample after annealing at 175°C for 30 min. The thickness of the sample increases from left to right. Selected area diffraction patterns showing that (b) most of the film is amorphous and that (c) the region in contact with the substrate has transformed into polycrystalline Pd_5InP with a preferred orientation to (d) the InP substrate.

The orientation relationship to the substrate is

$$(100)\ InP \parallel (001)\ Pd_5InP,$$

$$[011]\ InP \parallel [010]\ Pd_5InP.$$

During TEM examination the recrystallized band became wider, suggesting that the electron beam energy aided the recrystallization. The morphology suggests that the transformation was limited by the availability of nucleation sites. The amorphous film transformed to Pd_5InP in those areas in contact with the InP substrate and also in one patch a few μm in size far from the film/substrate interface.

EDS analysis was done at 19 points along a line through the polycrystalline patch and surrounding amorphous film. This profile is shown in Fig. 3.5. The average compositions of the patch and film are similar; $Pd_{5.5}InP_{0.7}$ and $Pd_{4.8}InP_{0.7}$, respectively. The statistical error in these measurements is less than 3.4% for Pd, 7.7% for In and 11.3% for P. As can be seen in the figure, the scatter in the data is more than twice the statistical error, indicating nonhomogeneity in both the amorphous and polycrystalline material. It should be noted also that for InP substrate material, EDS analysis gives a P:In ratio of 0.93. The electron beam focused on the specimen to collect EDS data causes preferential loss of P at the sampling site.

A cross-sectional view of this sample is shown in Fig. 3.6. The thickness of the overlayer is 60-70 nm, a first

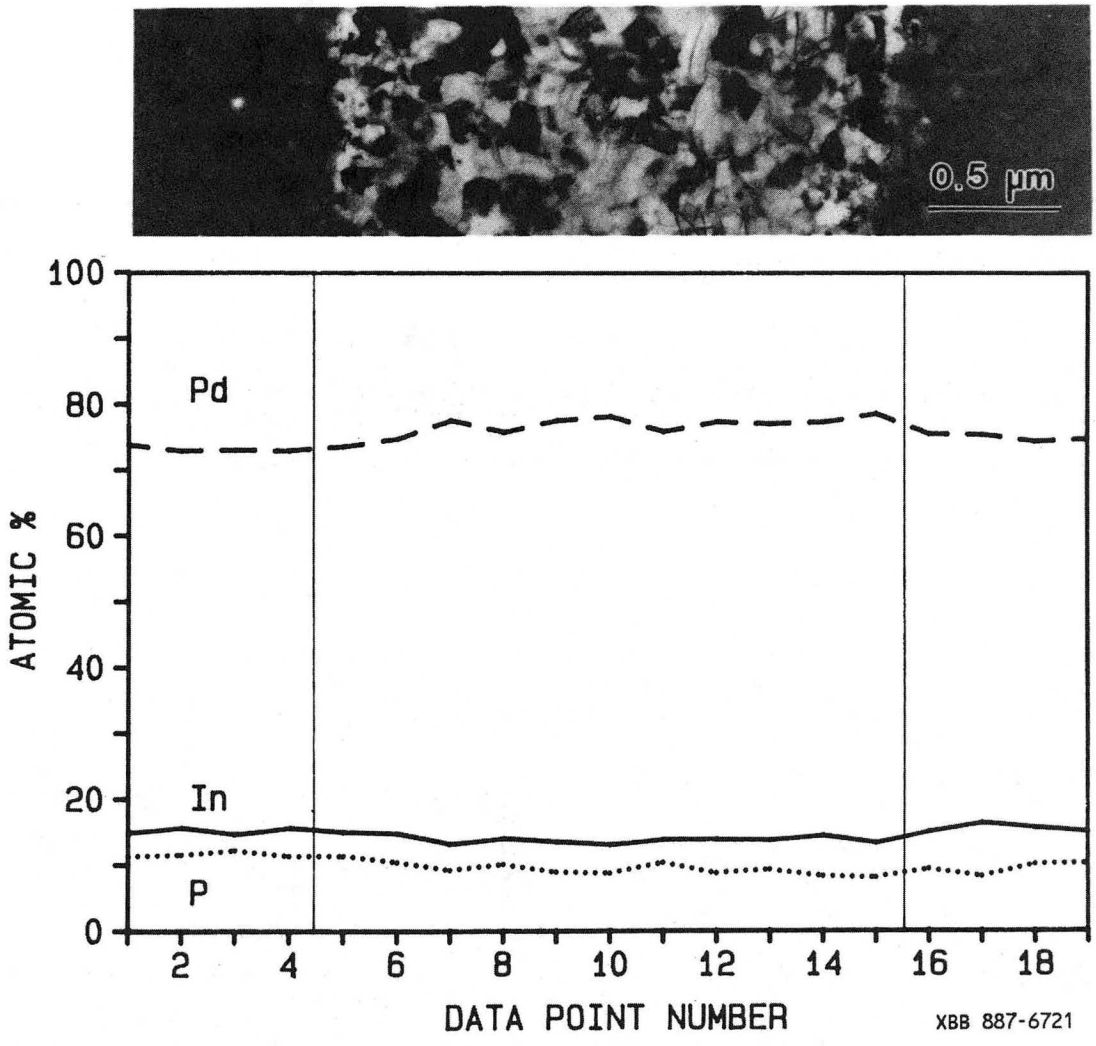

Figure 3.5 EDS data from Pd/InP sample annealed at 175°C for 30 min. Data was collected at 19 points along the polycrystalline patch and surrounding amorphous film in the region shown in the micrograph at top. Points 5 - 15 are from the polycrystalline patch. Points 1 - 4 and 16 - 19 are from the amorphous film.

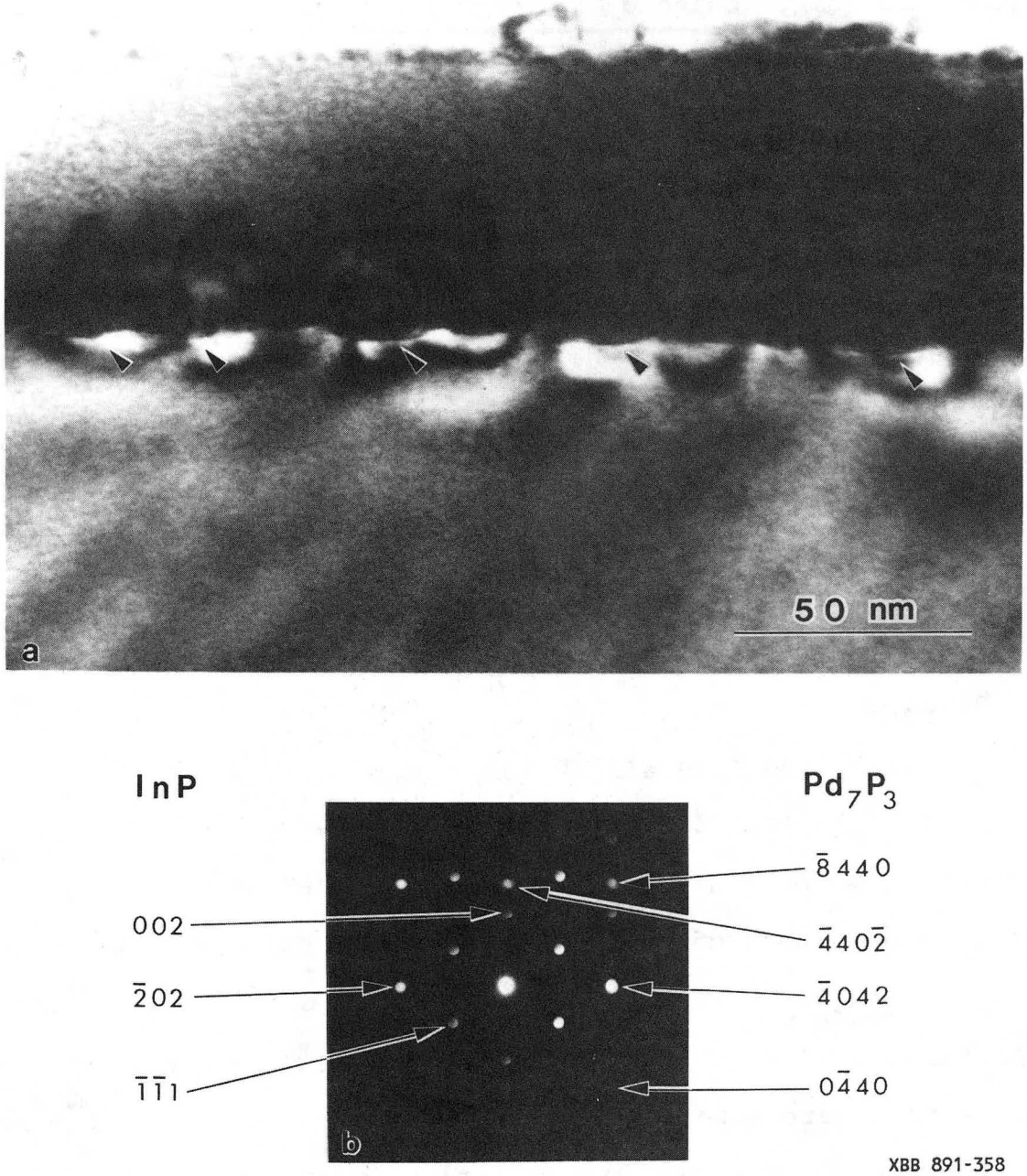

Figure 3.6 Cross-sectional TEM image of Pd/InP annealed at 175°C for 30 min. Most of the reacted layer is amorphous with a small amount of unreacted Pd at the surface. Strain contrast at the metal/semiconductor interface (marked with arrows) indicates nuclei of a new phase. The microdiffraction pattern is from the interface and shows InP spots, Pd_5InP amorphous rings, and spots from the new phase, Pd_7P_3.

indication that the 40-nm Pd layer has undergone a transformation. The bulk of the layer has homogeneous dark contrast that changed very little with specimen tilt, suggesting that the material is amorphous. At the top edge is a very thin, irregular layer that corresponds most likely to the Pd (or Pd-rich) layer detected by AES. At the InP interface there are many small particles on the order of 15 to 25 nm in size which are visible by moire fringe contrast. Strain contrast in both the adjacent InP substrate and reacted layer can be seen around these particles. The microdiffraction pattern shown in Fig. 6b is taken from this interface area and shows spots from both InP and another phase. The spots can be indexed as the [122] pole of the hexagonal phase Pd_7P_3 (a = 1.1976 nm, c = 0.7055 nm, c/a = 0.589).

3.1.3 Reaction at 215 and 250°C

Samples annealed at 215 and 250°C were similar to each other in morphology and composition. The reacted region of the sample annealed at 215°C for 30 min had the composition $Pd_{3.4}InP_{0.8}$, as determined by EDS analysis. Auger depth profiles were done for specimens both with and without SiO_2 caps that were annealed at 250°C for 30 min (Fig. 3.7). For the capped sample there was a Pd-rich surface and a continuous Pd_xInP (x = 3-5) layer. For the sample that had not been capped, there was enrichment of both indium and oxygen at the surface. Again a thick continuous layer of Pd_xInP followed.

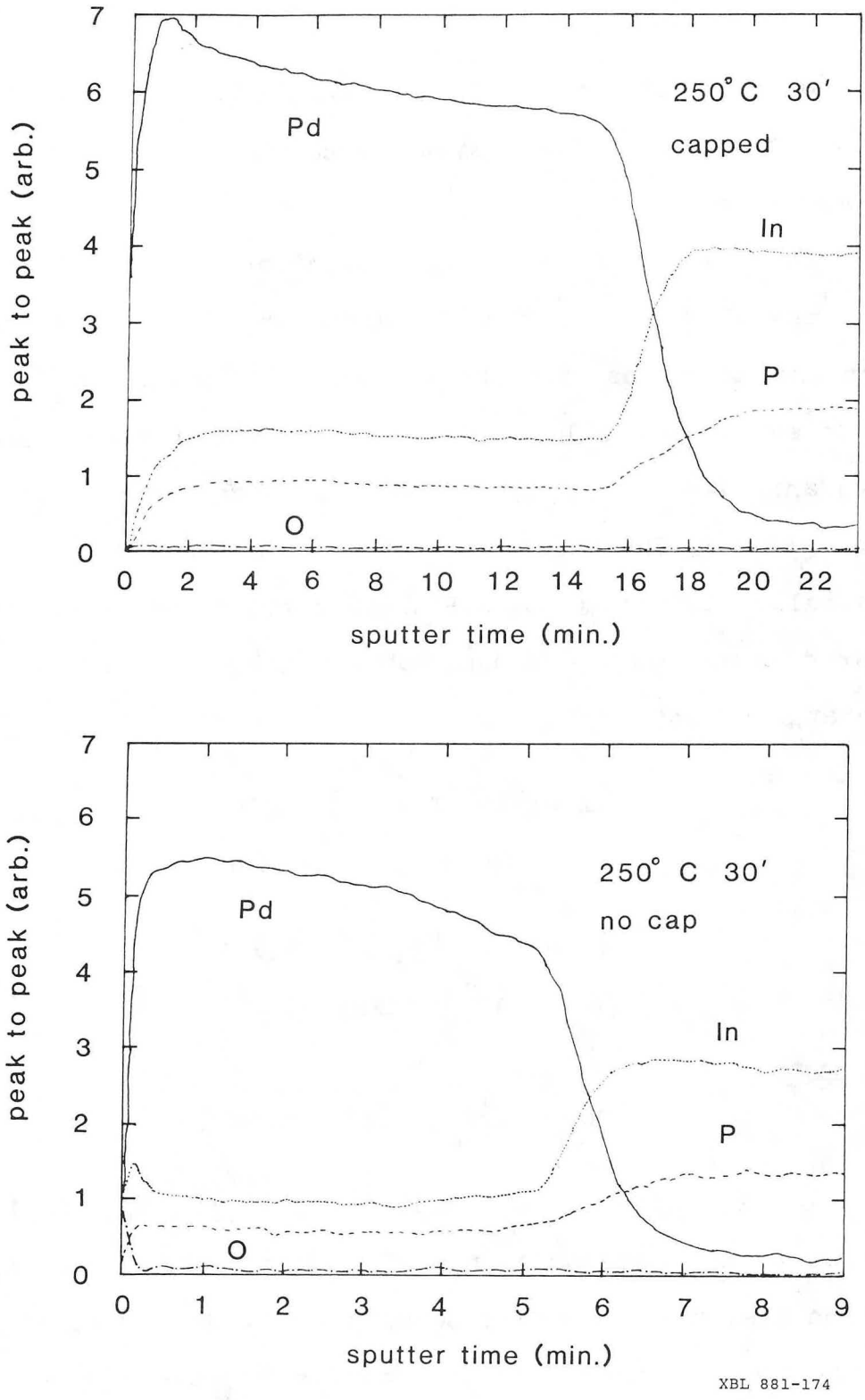

Figure 3.7 AES depth profiles of Pd/InP samples, with and without a SiO_2 cap annealed at 250°C for 30 min. At this temperature the cap is necessary to prevent the formation of surface oxides. For both samples the composition of the reacted layer below the surface is nearly constant with depth.

Here x was estimated to range from 4.5 to 5.5. Except for the peak at the surface, the oxygen concentration was below the AES detection limit.

Plan-view TEM of the 250°C specimen that had not been capped revealed a grain size of about 10 - 20 nm. In some of the thinnest regions, amorphous ring patterns were still found in this sample as well as in the 250°C capped sample and the sample annealed at 215°C, but over a large portion of these films, the diffraction patterns were crystalline and essentially the same (Fig. 3.8). Most spots can be attributed to three orientations of the tetragonal phase, Pd_5InP. The orientation relationships are

$$(100)\ InP \parallel (001)\ Pd_5InP,$$
$$[011]\ InP \parallel [010]\ Pd_5InP \text{ (as for 175°C)};$$

$$(100)\ InP \parallel (110)\ Pd_5InP,$$
$$[010]\ InP \parallel [\bar{1}10]\ Pd_5InP$$

and

$$[001]\ InP \parallel [\bar{1}10]\ Pd_5InP,$$

with a lattice mismatch of -5.3% to -5.4% for Pd_5InP planes, referred to the corresponding InP planes. These diffraction patterns also feature a diffuse ring with a d-spacing of 0.231 nm. This was present for all samples annealed from 215 to 650°C. The origin of this ring has not been determined. Oxides commomly associated with InP (In_2O_3, $InPO_4$) were

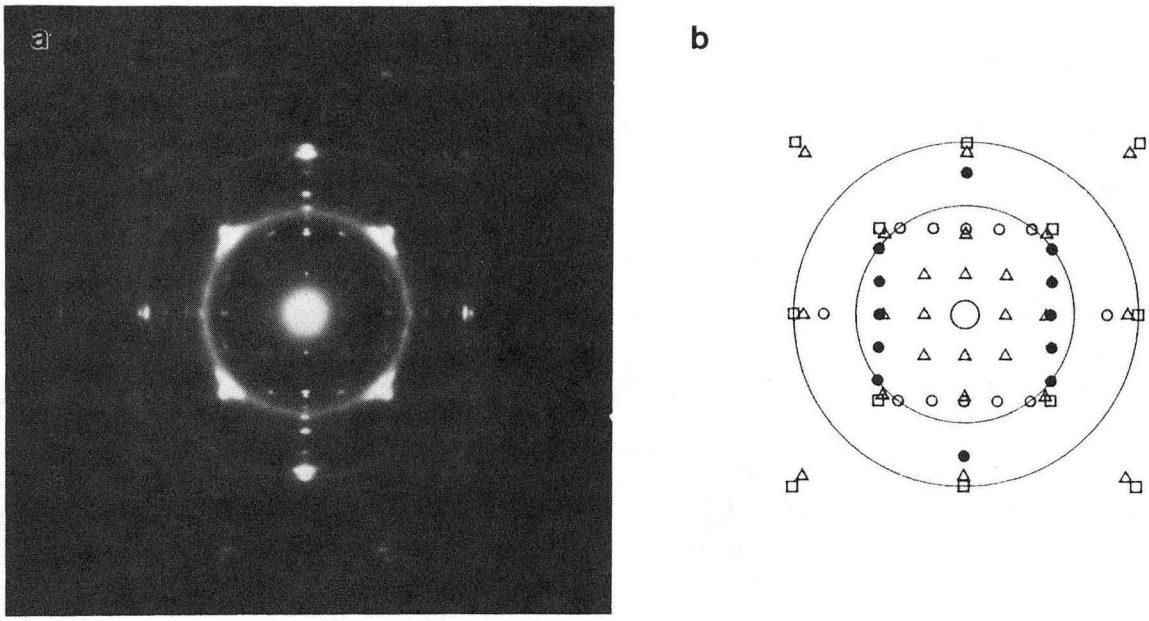

Figure 3.8 Electron diffraction pattern from Pd/InP sample annealed at 250°C for 30 min. (b) Indexing diagram: triangles indicate reflections from the InP [100] pole; squares are from the Pd_5InP [001] pole; and open and closed circles are two orientations of the Pd_5InP [110] pole.

considered. There is one match with the (211) plane of $InPO_4$ (d = 0.2326 nm), but this is not very convincing. The structure of this phase is orthorhombic, so it has very many plane spacings. One match is not conclusive.

The XRD spectrum for the capped 250°C sample showed a strong Pd peak. The most prominent new feature was a shoulder on the InP {200} peak at 2θ of 32°. This corresponds to a d-spacing of 0.280 nm, in good agreement with the Pd_5InP {110} plane spacing of 0.2778 nm.

3.1.4 Reaction from 450 to 650°C

The x-ray diffraction spectra of samples annealed from 450 to 650°C showed many new peaks not seen at lower temperatures; they were indexed as the simple cubic phase PdIn (a = 0.3260 nm). The intensities of these peaks increased with increasing annealing temperature.

The morphology of the reacted layer and electron diffraction patterns from samples annealed for 30 min at temperatures from 450 to 650°C were very similar to one another. The layer has agglomerated into islands with the largest ones ranging in size from 200 to 600 nm. The image and SAD pattern of the 650°C sample are shown in Fig. 3.9. The pattern shows PdIn reflections with strong texture; there are two dominant orientations. The orientation relationships are

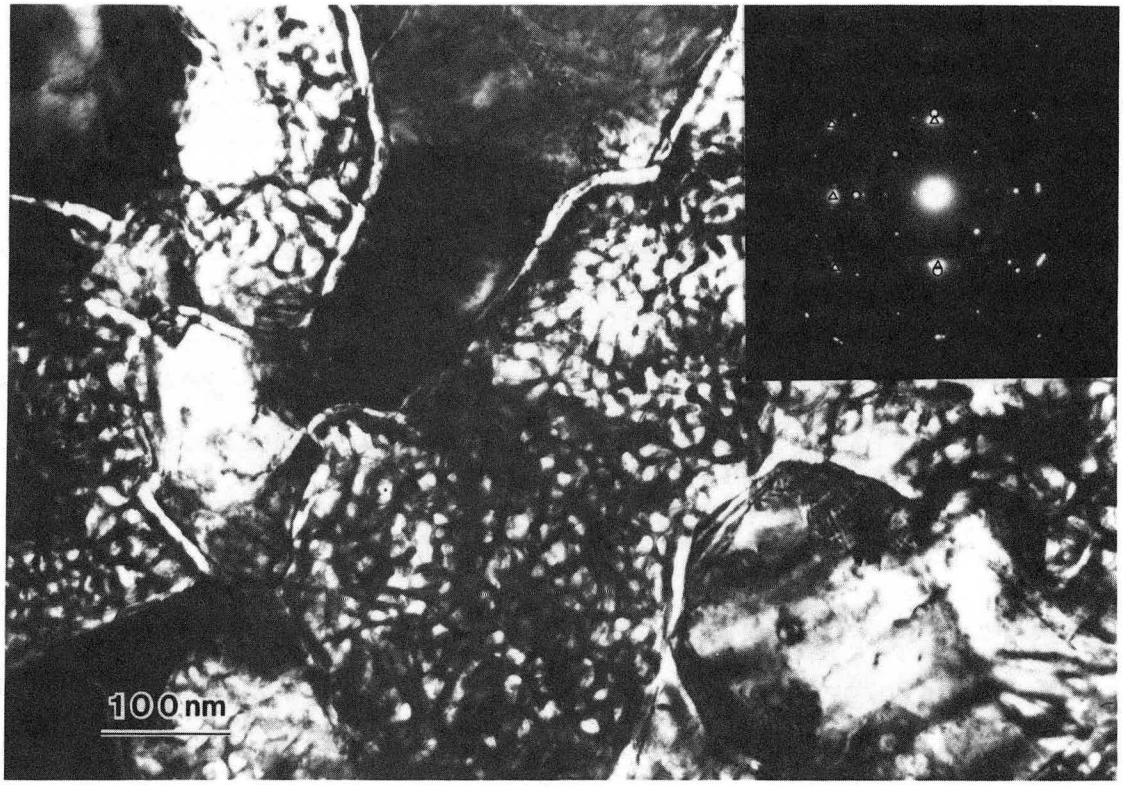

XBB 891-355

Figure 3.9 a) Plan-view image of Pd/InP annealed at 650°C for 30 min. b) Selected area diffraction pattern shows PdIn and InP reflections. Triangles indicate the [100] PdIn, and circles indicate the [100] InP poles.

(100) InP ‖ (100) PdIn,

[001] InP ‖ [001] PdIn;

and

(100) InP ‖ (110) PdIn,

[011] InP ‖ [$1\bar{1}0$] PdIn.

The lattice mismatch for these PdIn planes is of the order of -11%, referred to the corresponding InP planes.

Fig. 3.10 shows the image of the 650°C material viewed in cross-section, where the morphology can be seen even more clearly. The InP interface is very rough on a scale of about 60 nm. The large dark areas are PdIn. In some areas these are in contact with the InP substrate. In other areas there are voids or intervening regions of very low density material, which are visible also in regions between PdIn islands. Microdiffraction reveals that this material is amorphous. The two strongest rings correspond to interatomic distances of about 0.231 and 0.130 nm. The former is the same as the d-spacing of the diffuse ring mentioned earlier for all samples annealed from 215 to 650°C.

EDS results are inconsistent. The low density of these regions made it necessary to collect data for long periods of time. The diameter of the electron beam was similar in size to the areas of interest. Although the position of the beam was monitored and corrected during data collection small movements may have occured. Brief excursions of the beam into

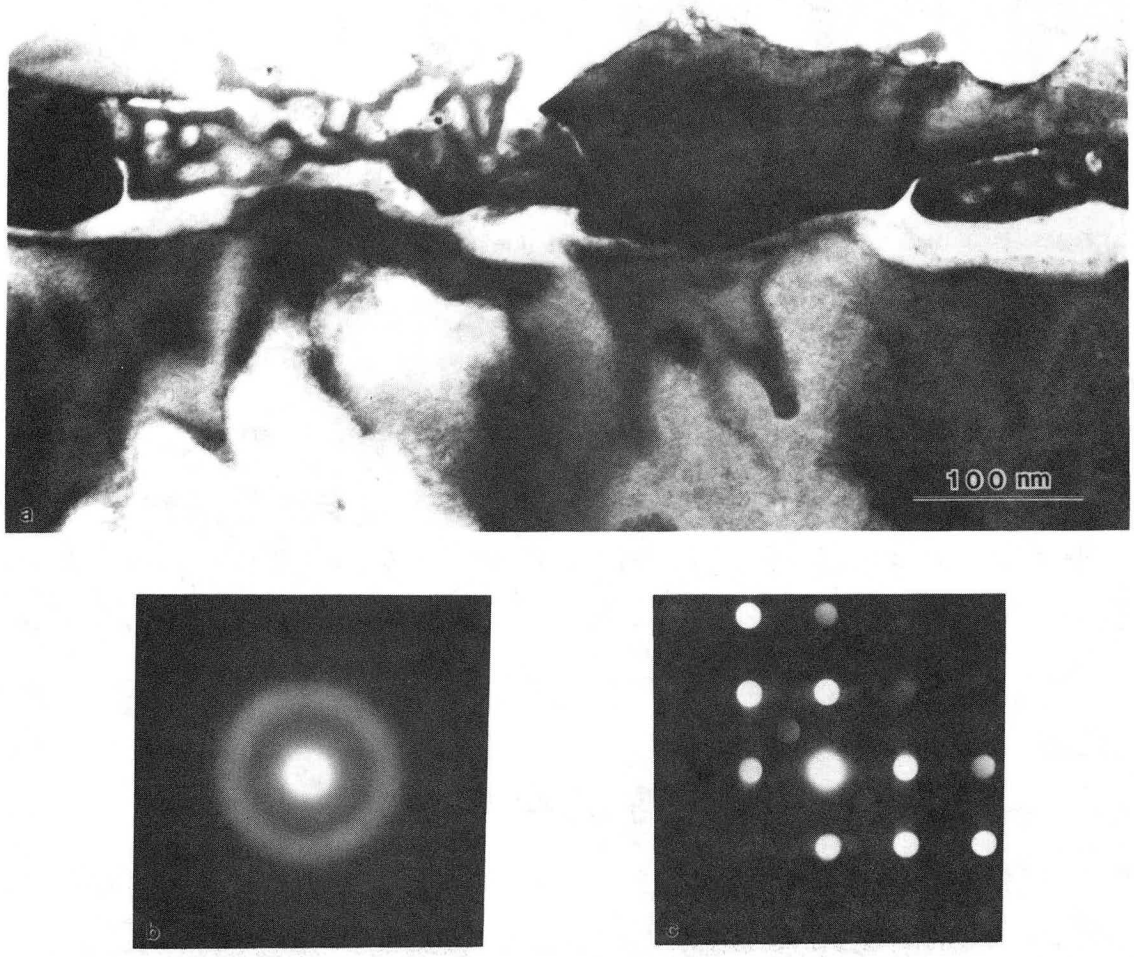

Figure 3.10 Pd/InP annealed at 650°C for 30 min shown in cross section (a). Microdiffraction reveals that the regions with many voids are amorphous (b) and that the darker regions are PdIn (c).

adjacent areas as well as spreading of the beam within the sample may have added significant contributions from the surrounding and much denser PdIn and InP.

Data collected from these samples using SBXRD are shown in Table 3.1. The strongest peaks agree well with d-spacings for PdIn. It is more difficult to draw conclusions about the other phases considered. The fact that $InPO_4$ matches well with almost all peaks is not persuasive. The orthogonal structure of this phase causes it to have very many plane spacings. It is difficult not to find agreement. Results from TEM show clearly that a large portion of the reacted layer is an amorphous phase that has not yet been identified. It is most likely that this would appear as two or three broad peaks. The only broad peak in this data corresponds to a plane spacing of 0.17157 nm. This agrees well with both $InPO_4$and PdP_3. On the other hand, the strong peak at d = 0.22814, although sharp near the top, broadens out considerably at its base before blending with the background signal. This could be a super-position of the sharp PdIn 110 peak and a broad amorphous peak corresponding to the 0.231 nm spacing seen in electron diffraction. This spacing finds reasonable agreement with both $InPO_4$ and In_2O_3.

3.2 Discussion

3.2.1 Low Temperature Phases

In recent years there have been reports of solid-state amorphization reactions (SSAR), where diffusion between films

TABLE 3.1

40 nm Pd/InP 450°C[a] or 650°C[b] 30 min

Seemann-Bohlin X-Ray Data

Plane spacings	$InPO_4$	In_2O_3	PdP_3	PdIn
0.22814[a,b]	0.2262 (003)	0.2262 (420)		0.2305 (110)
0.17157[a,b]	0.1716 (301)		0.1723 (420)	
0.13211[a,b]	0.1317 (323)		0.1321 (530)	0.1331 (211)
0.12069[b]	0.1209 (035)		0.1219 (620)	
0.12018[b]				
0.11943[a,b]	0.1195 (215)	0.1192 (660)	0.1189 (541)	
0.11454[a]	0.1144 (343)		0.1136 (631)	0.1153 (220)
0.10261[a]	0.1022 (450)			
0.09365[a,b]				0.0941 (222)

Note: All plane spacings are given in nm.
The strongest peak also matches the {422} plane spacing for InP (d = 0.1198 nm).

of certain crystalline metals results in formation of amorphous phases. Systems that behave in this way include Au-La,[43] Au-Y,[44] Ni-Zr,[45] Cu-Zr,[46] Ni-Hf,[47] Co-Zr,[48] Sn-Co,[49] Fe-Zr,[50] and Ni-Ti.[51] These investigators concluded that the reaction is driven by the large negative heat of mixing of the two components and occurs over a broad range of compositions centered near a minimum in the free energy curve. Another essential factor is the fast diffusion of one component in the other. Amorphous phase growth is diffusion-limited and will proceed as long as the annealing temperature is high enough to allow diffusion and low enough to avoid nucleation of crystalline phases. Although the crystalline phases are more stable thermodynamically, they are kinetically improbable at these temperatures. Amorphous phase formation starts preferentially at incoherent or disordered interfaces or, better yet, grain boundary triple points[52]. For a comprehensive treatment of SSAR, the reader is referred to the review article by W.L Johnson.[53]

Ternary Zr-M-H systems (zirconium-based hydrides) have also shown SSAR behavior.[54,55] Analysis of these systems provides insight that can be applied to the Pd/InP system. The thermodynamic considerations for both binary and ternary systems are the same, but often, thermodynamic data is not available for the ternary systems of interest. Free energy calculations are not possible. For the Zr_3Rh-H system Yeh, et al.[56] describe a "chemical frustration" effect as the

underlying mechanism for the transition to the amorphous state. In hydriding crystalline Zr_3Rh, a two-phase equilibrium reaction product containing ZrH (or ZrH_2) and a Rh-rich phase is expected. Hydrogen is highly mobile at SSAR temperatures (< 200°C), but Zr and Rh are not. The restricted interdiffusion of Zr and Rh precludes formation of nuclei of the stable phases. Transformation to the amorphous hydride ($Zr_3RhH_{5.5}$) is a metastable alternative that does not require diffusion of the metal species.

A diagram summarizing the Pd/InP results is shown in Fig 3.11. The low temperature reaction begins with formation of an amorphous ternary phase. Analogies to the Zr-M-H systems can be made. Based on Si-M binary couple reactions, Walser and Bene[57] predict that the first crystalline phase nucleated is the most stable (i.e., highest melting temperature) congruently melting compound next to the lowest-temperature eutectic on the bulk equilibrium phase diagram. In the absence of a ternary phase diagram for this system the In-Pd and Pd-P binary phase diagrams (as shown in Fig 3.12) are used as guides. The first phases expected are Pd_7P_3 or Pd_3P and PdIn. Although Pd can diffuse readily into the substrate, the In and P atoms are relatively immobile at these temperatures. Segregation of the In and P species into a two-phase mixture is not possible, and "chemical frustration" occurs. The Pd breaks In-P bonds, resulting in a transformation to metastable amorphous Pd_5InP. Crystallization of this phase at

As-Deposited
Interdiffusion of Pd and InP begins upon deposition.

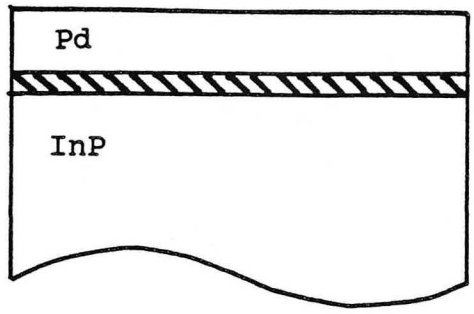

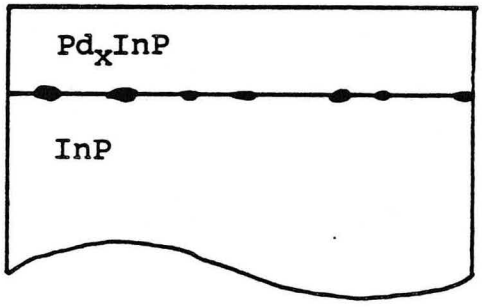

175°C 30 min
Reacted layer is amorphous Pd_xInP. Nuclei of Pd_7P_3 appear at interface with InP.

250°C 30 min
The amorphous ternary phase has crystallized into tetragonal Pd_5InP. No Pd_7P_3 is found.

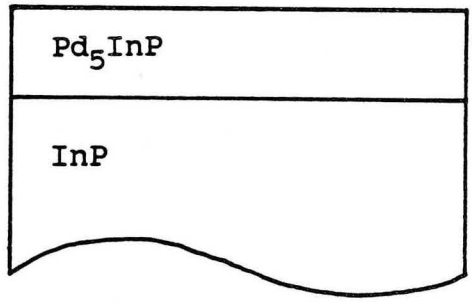

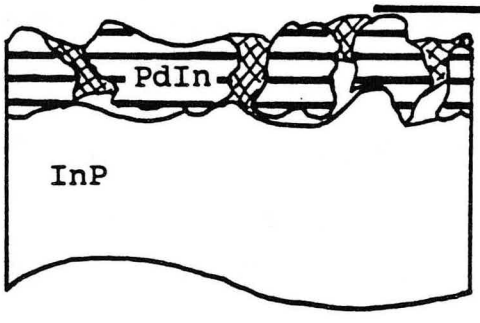

450°C 30 min
Reacted layer has irregular morphology. Islands of PdIn are interspersed with voids and oxide regions.

650°C 30 min
Coarser version of morphology seen at 450°C. PdIn islands, voids, and oxide regions are all larger.

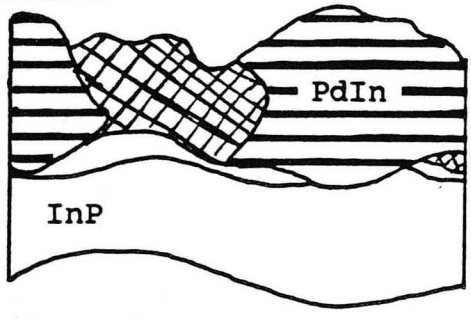

Figure 3.11 Schematic drawing summarizing the results of the Pd/InP study.

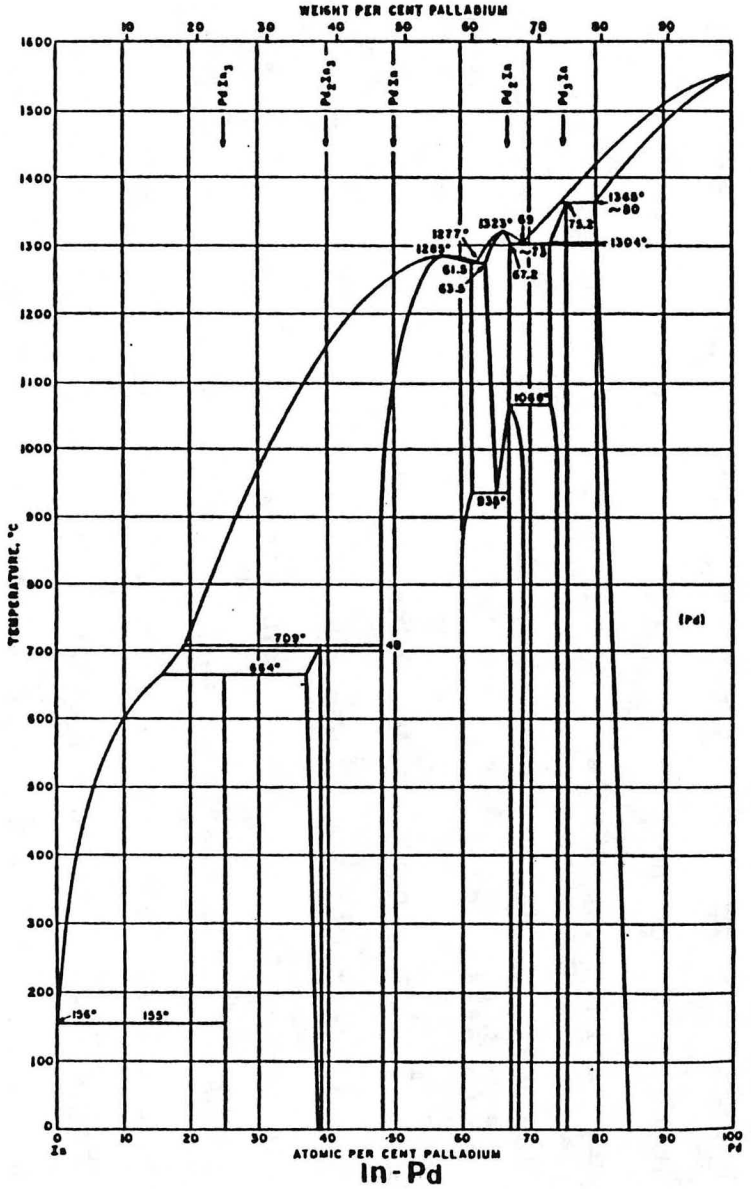

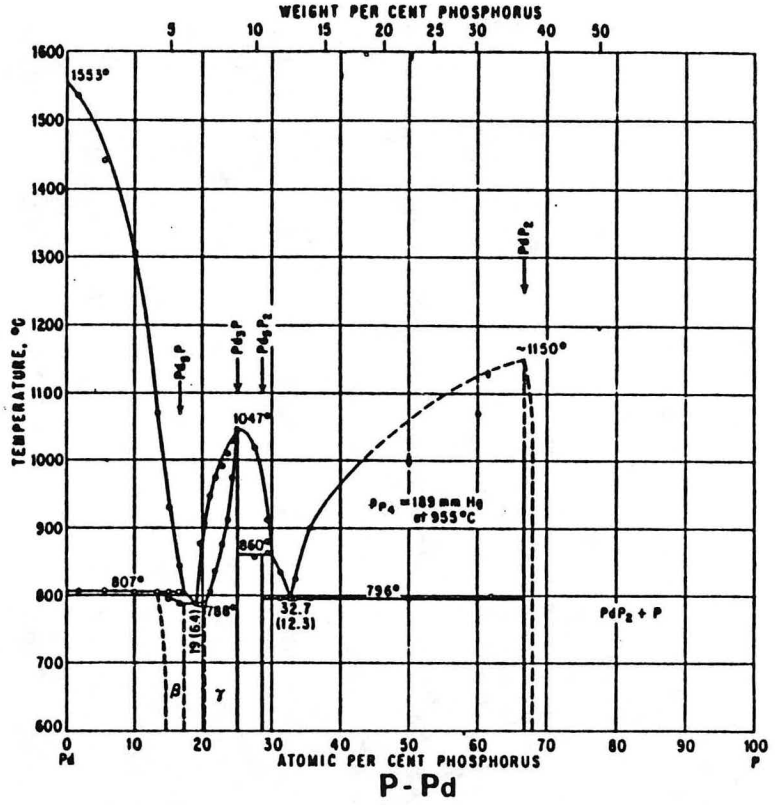

Figure 3.12 In-Pd[58] and P-Pd[59] binary phase diagrams.

heterogeneous nucleation sites (at 175°C) and at slightly higher annealing temperatures (215°C) suggests that there may be a ternary phase of this composition on the equilibrium phase diagram. Further evidence for this can be found in the work of El-Boragy and Schubert[60] who worked out the 600°C isotherm of the Pd-In-As phase diagram and found a ternary phase of composition Pd_5InAs. They identified a number of other Pd-based ternary phases with the same structure. Among these is $Pd_{72}In_{14}P_{14}$ (Pd_5InP), found after annealing at 600°C for one day.

At 175°C, crystallization of Pd_5InP may have to compete with growth of the Pd_7P_3 phase which nucleates at the InP interface, although it is likely that Pd_7P_3 is unstable with respect to Pd_5InP above this temperature. No evidence of Pd_7P_3 was found after higher temperature anneals. But it is important to note that for the 175°C anneal, Pd_5InP crystallization was facilitated by the electron beam in TEM. Perhaps further annealing at 175°C would have resulted in growth of the Pd_7P_3 phase.

Similar behavior has been observed for Ni on InP where Sands[61] reported the first phase formed (at 200°C) as amorphous $Ni_{2.7}InP$. Other investigations (including this one) have not found this phase. There seem to be many factors involved in phase formation in this system. This will be discussed in Chapter 4. For Pd on GaAs[62,63] the initial low-temperature product is an intermediate crystalline phase. Amorphous phases

have not been observed during transition-metal/GaAs reactions.

3.2.2 High Temperature Phases

Identification of PdIn accounts well for the Pd and In in the samples annealed at temperatures from 450 to 650°C, but raises the question of what happened to the P. A similar result has been reported for Pd/GaAs, where at 400°C and higher the only reaction product was PdGa[64]. In that case the sample had not been capped but was in direct contact with the annealing ambient, allowing preferential loss of volatile As. The Pd/InP samples annealed at these temperatures were protected by SiO_2 caps, but examination of these samples with a scanning electron microscope after annealing revealed a number of cracks and scrapes in the caps as well as areas of incomplete coverage. Although the caps did provide some protection, especially at lower temperatures (e.g., 250°C), they may not have been able to prevent preferential loss of P above 450°C. The InP (100) surface evaporates congruently up to 365 ± 5°C. Above this temperature there is a disproportionate loss of P_2 from the surface.[65] Other researchers who have used SiO_2 caps for InP annealing have reported dramatic cap failure due to cracking at 650[66] and 700°C[67]. Other studies suggest that some phosphorus loss may occur through 350-nm SiO_2 caps at temperatures from 450 to 650°C.[68]

Wilmsen and co-workers[69,70,71,72,73] have studied the thermal oxidation of InP using x-ray photoelectron spectroscopy and

other methods and have developed a model as follows: At 400°C $InPO_4$ is the initial oxide layer. For temperatures less than 600°C this acts as a diffusion barrier to P but allows passage of In. Whatever P does manage to get to the surface either evaporates or reacts to form more $InPO_4$. More In than P reaches the surface. The excess In reacts to form In_2O_3. The final result is an inner layer of $InPO_4$ with an outer layer comprising both $InPO_4$ and In_2O_3. For temperatures less than 650°C both of these are noncrystalline.

It is most likely that the amorphous phase observed from 450 to 650°C in this study is $InPO_4$. In Wilmsen's model, In_2O_3 is formed because there is excess In available for reaction with oxygen. At these temperatures in the Pd/InP system, PdIn forms readily, thus removing the excess In and preventing formation of In_2O_3. The reaction can be described by:

$$2InP + Pd + 2O_2 \rightarrow PdIn + InPO_4 + P\uparrow.$$

3.3 Conclusions

It has been shown that the reaction between Pd and InP begins at room temperature and is insensitive to the InP native oxide. The first phase forms a flat interface with InP and is an amorphous ternary phase of approximate composition Pd_5InP. This phase persists after annealing at 175°C and crystallizes after further annealing at 215°C. At temperatures from 450 to 650°C, the morphology is very rough

and globular, and the only phase identified is PdIn. Phosphorus is so volatile at these temperatures that it is difficult to maintain a closed system in spite of SiO_2 caps on the samples.

Pd shows some promise as a metal contact component for InP devices for temperatures up to at least 250°C. The low-temperature, ternary phase contains equal amounts of In and P, has a uniform, regular morphology, and forms easily in spite of the InP native oxide; all desirable metallurgical properties for a contact material.

The next chapter will discuss Ni reactions with InP and evaluate the usefulness of this metal as a component for device contacts.

CHAPTER 4

4. Ni/InP System

4.1 Experimental Results

4.1.1 As-Deposited

4.1.1.1 Deposition 1 (100 nm)

A 100-nm layer of Ni was deposited onto an InP wafer that had undergone the standard cleaning. It was cut into pieces for subsequent annealing. A full description of these procedures can be found in Section 2.1.2.

In preparing a cross-section specimen for TEM, this material was exposed to a temperature of about 100°C for 1 hr. The image from this specimen in Figure 4.1 shows a 5-nm interfacial layer between the polycrystalline Ni overlayer and the InP substrate. This layer looks similar to that seen for as-deposited Pd/InP in Figure 3.2, which suggests that this also may be an amorphous ternary phase. There is no apparent oxide layer at this interface.

4.1.2 Reaction at 240°C

4.1.2.1 Deposition 1

A sample from deposition 1 was annealed at 240°C for 30 min in flowing Ar-5%H_2 gas. Examination by RBS showed that no more than 10 nm of the Ni had moved into the InP substrate. This had not been expected since the start of the reaction had already been observed in the as-deposited sample. Reports in the literature have shown Ni/InP reactions at temperatures as

XBB 891-354

Figure 4.1 Cross-sectional TEM image of Ni(100 nm)/InP sample as-deposited. Much of the original polycrystalline Ni layer has been milled away during specimen preparation. An interfacial reacted layer approximately 5 nm in thickness is visible. No InP native oxide is apparent.

low as 200°C (see Table 4.3).

4.1.2.2 Deposition 2 (74 and 32 nm)

Another set of Ni depositions was done. These samples were designed to test the effects on the reaction products of 1) different etchants in the surface preparation of the InP wafer and 2) the thickness of the Ni layer. Three samples were made. All wafers were prepared using the standard cleaning procedure. Two wafers underwent an additional step of etching in H_2O:HF (9:1) for 2 min. On one of these, a thick layer of Ni (74 nm) was deposited; the other received a thinner layer (32 nm). A 32-nm layer of Ni was deposited also on the wafer that had undergone only the standard cleaning procedure. In this scheme, Deposition 1 completes the set as a wafer cleaned in the standard way with a thick (100 nm) layer of Ni. Details of these procedures are discussed in Section 2.1.2.

In samples annealed at 240°C for 30 min in flowing Ar-5%H_2, RBS showed that about 20 nm of the Ni had been consumed. An interfacial layer was formed with nominal composition Ni_3InP. In the XRD spectrum the strongest peak (apart from the InP peaks) is broad and corresponds to a plane spacing of 0.1918 nm. Sands, et al.[74] found an amorphous ternary phase with an interatomic distance of 0.21 nm after annealing at 200°C for 15 min. This is almost 10% larger than the value found here. There is better agreement with the 0.1895 d-spacing of the {111} planes in the hexagonal $Ni_{2-3}InP$ phase (a

= 0.4120, c = 0.4830). The phase in the present study may be partially transformed $Ni_{2-3}InP$. However, this must be regarded as a preliminary identification.

No effect due to either the etchant or the Ni layer thickness was found. All samples in Depositions 1 and 2 gave similar results, regardless of InP etchant or Ni layer thickness.

4.1.3 Reaction at 275°C

4.1.3.1 Deposition 1 (100 nm)

Samples were annealed at 275°C for 30 min in Ar-5%H_2, N_2-4%H_2, or in N_2-4%H_2 with a polished InP wafer placed face down on the Ni film to reduce the loss of volatile, P-containing species. These different annealing ambients seemed to have no effect; the results were the same for all.

As shown in Fig. 4.2a, RBS revealed a layered structure with a P-rich phase of composition Ni_2P next to the substrate and an In-rich phase of approximate composition In_4Ni_3 near the surface.

Over the InP substrate, cross-sectional TEM (Fig. 4.3) showed two distinct and well-defined layers separated by an intervening layer 2 to 4 nm in thickness. The contrast from the intervening layer was very bright and did not change with angle of tilt under the electron beam. Using micro-diffraction, the outermost layer, layer 1, was found to be polycrystalline and layer 2, adjacent to the substrate, to be epitaxial. Lattice plane spacings from layer 1 agree well

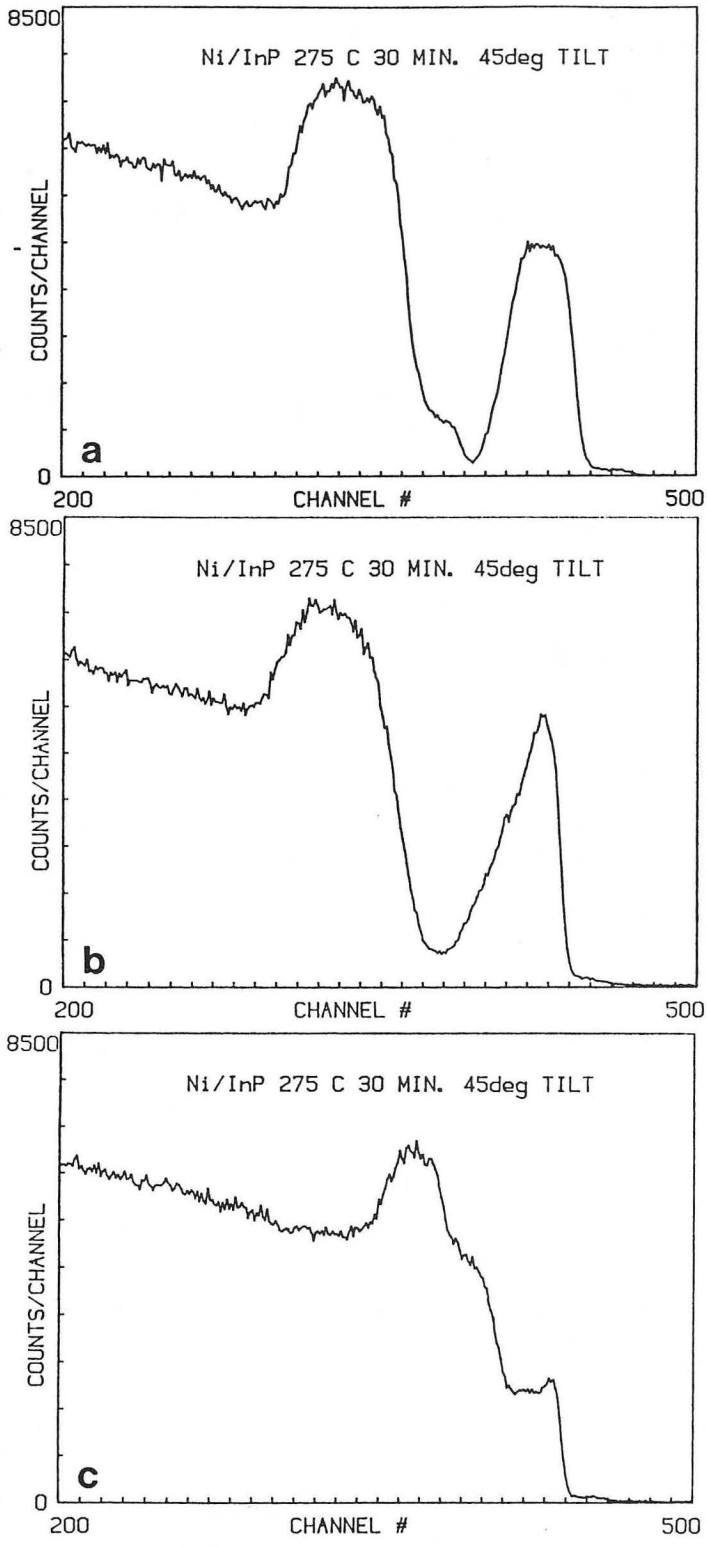

Figure 4.2 RBS spectra for Ni/InP samples annealed at 275°C for 30 min. Segregation of In to the surface and P to the substrate is less pronounced as the thickness of the Ni layer decreases from (a) 100 to (b) 74 to (c) 32 nm.

XBB 891-359

Figure 4.3 Cross-sectional TEM image of a Ni(100 nm)/InP sample annealed at 275°C for 30 min shows a very distinct layered structure. Microdiffraction patterns in insets identify the top layer (layer 1) as polycrystalline In_3Ni_2 and the layer adjacent to the InP substrate (layer 2) as epitaxial Ni_2P.

with several phases. The most likely ones are monoclinic $In_{21}Ni_{29}$ (In_3Ni_4) with a = 1.4646, b = 0.8329, and c = 0.8977 nm and hexagonal In_3Ni_2 with a = 0.4396 and b = 0.5210 nm. Layer 2 is hexagonal Ni_2P (a=0.5864, c=0.3385 nm, c/a=0.5773). There is an epitaxial relation between Ni_2P and InP with the following orientation relationship:

$$(100)\ \mathrm{InP} \parallel (1\bar{2}11)\ Ni_2P$$
$$[110]\ \mathrm{InP} \parallel [01\bar{1}2]\ Ni_2P,$$

and a lattice mismatch of 22% referred to the corresponding InP planes.

The plane spacings determined by XRD and d-spacings of candidate phases are shown in Table 4.1. There is agreement with In_3Ni_4, In_3Ni_2 and Ni_2P. There are additional plane spacings that cannot be attributed to any of these phases. In light of the RBS data the In-Ni phase is most likely In_3Ni_2.

4.1.3.2 Deposition 2 (74 and 32 nm)

After the 240°C samples were annealed a second time at 275°C for 30 min all the Ni was consumed, and within the reacted layer there was strong segregation of In to the surface and of P to the substrate (Fig 4.4a). Samples that had undergone only one heat treatment at 275°C showed a similar result, although the segregation was less pronounced (Fig 4.4b). In Figure 4.2, comparison of the three Ni layer thicknesses, all annealed at 275°C for 30 min, shows that

TABLE 4.1

Ni/InP 100 nm Deposition 1 275°C 30 min

XRD plane spacings	InP	Ni_2P	In_3Ni_4	In_3Ni_2
0.3069 nm				0.3074 nm (101)
0.2931	0.2934 nm (200)	0.2932 nm (110)		
0.2468			0.2448 nm ($20\bar{1}$)	
0.2276				
0.2212		0.2216 (111)	0.2204 (022)	0.2198 (110)
0.2077			0.2082 (040)	
0.1933			0.1933 (041)	
0.1918		0.1919 (120)	0.1912 ($30\bar{1}$)	0.1904 (200)
0.1467	0.1467 (400)	0.1466 (220)	0.1465 ($42\bar{1}$)	

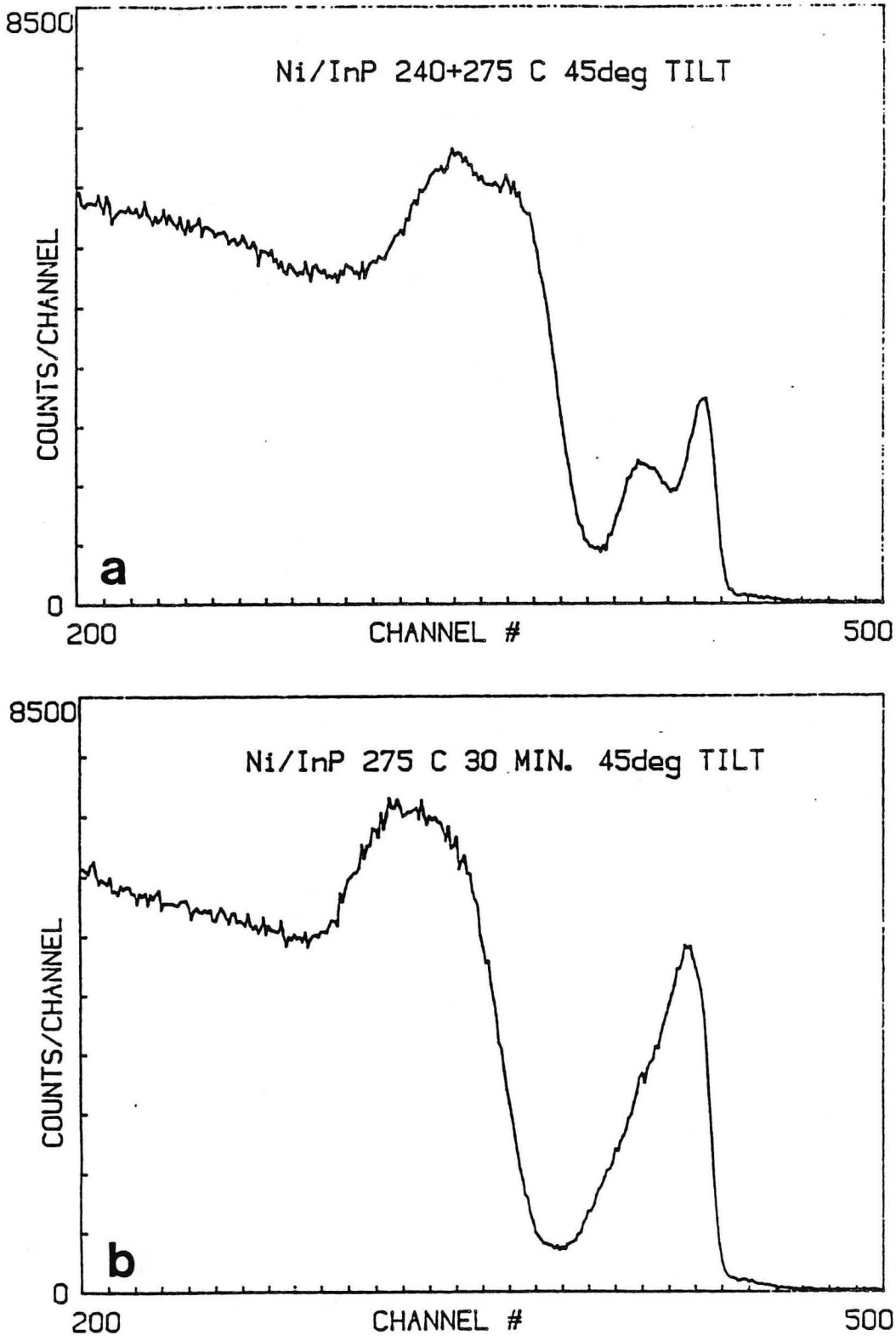

Figure 4.4 RBS spectra for Ni(74 nm)/InP samples annealed (a) at both 240 and 275°C and (b) at 275°C alone. The two-step annealing process results in enhanced In and P segregation.

segregation of In and P increases as a function of thickness.

The XRD spectrum from a sample annealed at 275°C for 30 min yielded the plane spacings listed in Table 4.2. The strongest peaks correspond to the d-spacings that are underlined. There is good agreement with Ni_2P and many matches with both Ni_2InP and In_3Ni_4, but it is difficult to interpret these last two. They are both monoclinic phases and, therefore, have very many d-spacings, so the likelihood of finding agreement is much higher than, for example, with a cubic phase. In addition, the positions of the atoms in the Ni_2InP structure are not known, so its diffraction extinction conditions cannot be taken into account. There is only fair agreement with In_3Ni_2 .

A sample with a 32-nm Ni layer annealed at 275°C for 30 min was examined in TEM in plan view. Polycrystalline rings, spot patterns and amorphous rings were seen. The polycrystalline rings index as Ni_2InP, the spot patterns as Ni_2P, and the amorphous areas as $InPO_4$. It is not possible to say whether the oxide was at the specimen surface or within the reacted region.

4.1.4 Reaction at 600°C

4.1.4.1 Deposition 1

A sample from deposition 1 (100 nm Ni layer) that had been annealed at 275°C was capped with 200 nm of SiO_2 and annealed again at 600°C for 60 min to assess the stability of the layered structure. A cross-section sample was examined

TABLE 4.2

Ni/InP 74 nm Deposition 2 275°C 30 min

XRD plane spacings	InP	Ni_2P	In_3Ni_4	Ni_2InP
0.6371 nm				0.6376 nm
0.3969				
0.2931	0.2934 nm	0.2932 nm		
0.2722				0.2730
0.2637			0.2638 nm	0.2645
0.2462				0.2464
0.2304				0.2297
0.2212		0.2216	0.2204	0.2209
0.2171				0.2162
0.2132			0.2143	0.2130
0.2023			0.2003	0.2025
0.1937			0.1933	0.1936
0.1918		0.1919	0.1912	0.1920
0.1684			0.1685	0.1687
0.1623			0.1625	0.1623
0.1600		0.1606	0.1599	0.1597
0.1544			0.1562	0.1545
0.1508		0.1514		0.1506
0.1467	0.1467	0.1466	0.1465	0.1470
0.1280			0.1279	0.1276
0.1151			0.1140	0.1149

in TEM. The phase adjacent to the InP substrate was identified as Ni_2P using microdiffraction. This composition was confirmed by EDS. In some areas, isolated agglomerations of Ni_2P were found on top of the otherwise exposed InP substrate. Although no other phase was found, the condition of the specimen suggested that if there were another layer, it may have been removed during specimen preparation.

4.2 Discussion

The results of this study and earlier studies by Appelbaum, et al.[75,76] and Sands, et al.[77] are summarized in Table 4.3. Appelbaum and co-workers found different results for different annealing ambients. With heat treatments in He, these investigators found no reaction for 100 nm Ni on InP after 200°C for 60 min. The Ni began to react with the InP at 250°C. After heat treatments of 60 to 90 min, In was found only in the surface and central regions of the film, P near the substrate, and Ni throughout. After heating at 300°C for 30 min, they found the following layered structure: $InNi_2/Ni_2P/InP$. Further annealing at 400°C resulted in oxygen and indium at the surface and Ni_3P throughout the bulk of the layer. For annealing in Ar-10%H_2, they found a fairly uniform Ni-In-P layer throughout the reacted region at 250°C and a single cubic ternary Ni_xIn_yP phase with a = 0.57 nm at 300 to 400°C. The study by Sands, et al. reported that for a 40-nm Ni film annealed at 200°C for 60 min, all Ni was consumed, and the resulting ternary amorphous phase had nominal composition

TABLE 4.3 Summary of Ni/InP REACTIONS

Conditions	This Work Deposition 1	This Work Deposition 2	Appelbaum[78,79]	Sands[80]
Oxide etch	$H_2SO_4:H_2O_2:H_2O$ (5:1:1) 2 min	$H_2SO_4:H_2O_2:H_2O$ (5:1:1) 2 min	H_2O:HF(10:1) 60 sec	$H_2SO_4:H_2O_2:H_2O$ (5:1:1) 2 min
Thickness	100 nm	30 or 74 nm	100 nm	40 nm
Annealing ambient	Ar-5%H_2 or N_2-4%H_2	Ar-5%H_2	Ar-10%H_2 or *He	N_2-5%H_2
Heat treatment and result			*200°C 60min no reaction	200°C 15min 20nm Ni reacted; 60min $Ni_{2.7}InP$ amorphous
	240°C 30min 10nm Ni reacted	240°C 30min 20nm Ni reacted $Ni_{2-3}InP$ hexagonal?	250°C 30, 60 or 90 min Ni-In-P *250°C 60 or 90 min In-Ni/ Ni-P/InP	250°C 15min $Ni_{2.7}InP$ amorphous
	275°C 30min $In_3Ni_2/Ni_2P/InP$	275°C 30min In_3Ni_4?/ $Ni_2InP/Ni_2P/InP$	300-400°C Ni_xIn_yP cubic	300°C 15min $Ni_{2-3}InP$ hexagonal
			*300°C 30min $Ni_2In/Ni_2P/InP$	360°C 60min or 500°C 15min Ni_2InP monoclinic
	600°C 60 min ?/Ni_2P/InP		*400°C 10min O/In/Ni_3P/InP	
Analysis used	RBS, XRD, TEM	RBS, XRD, TEM	RBS, AES, XRD	TEM, AES, EDS

$Ni_{2.7}InP$. This phase persisted through a short 250°C anneal. It transformed to hexagonal $Ni_{2-3}InP$ after 15 min at 300°C. Samples with no previous heat treatment that were annealed at either 360 or 500°C contained yet another ternary phase: monoclinic Ni_2InP.

4.2.1 Surface Oxide Effect

In their study to determine the In-P-O phase diagram, Schwartz, et al.[81] reported that the InP native oxide film comprises a single phase - $InPO_4$. Nelson and co-workers[82] reported that when InP is oxidized at temperatures from 400 to 600°C the $InPO_4$ layer grows. As it thickens, elemental P collects at the interface, and the outer layer becomes a mixture of In_2O_3 and $InPO_4$. They suggest that in this temperature range the $InPO_4$ inner layer acts as a diffusion barrier for P but not for In. The permeability of the native oxide on the substrate surface can also influence phase formation in thin film systems.

It is not clear that the surface oxide has any role in this study. Singh and co-workers[83] have shown that both oxide etching solutions in Table 4.3 are equally effective in reducing oxygen and carbon contaminations to levels lower than that of air-cleaved InP. (Both also leave a surface that is richer in In than P by about 2 to 1.) Whereas Sands, et al. had seen the initial reaction completed after annealing at 200°C for 60 min, in this study there was not much Ni diffusion even after 30 min at 240°C. (The results of

Appelbaum, et al. from He ambient samples are similar.) If there were a thick oxide layer at the InP substrate surface in this study it could have delayed the onset of interdiffusion, thereby increasing the temperature at which the first reaction occurs. Such a layer could have allowed only In to diffuse out to react with Ni and Ni to diffuse in to react with the accumulated P. If the layer sandwiched between the Ni-P and In-Ni phases is the original InP surface oxide, the reason for the $In_3Ni_2/Ni_2P/InP$ structure in Figure 4.3 would be clear. But the as-deposited specimen in Figure 4.1 shows nothing to suggest a thick native oxide on the substrate.

4.2.2 Metal Thickness Effect

In studies of M/GaAs systems, Sands and co-workers[84] have described an effect whereby the final phase or phase distribution is influenced by the original metal film thickness. For a very thin Pd layer (12 nm) on GaAs they reported the intermediate Pd_5Ga_2As phase as the dominant reaction product at temperatures as high as 600°C. For a thick Pd film (60 nm) the same ternary phase forms at about 275°C, but at higher temperatures the binary phases, PdGa and $PdAs_2$ were found. They attribute this difference to the large surface-to-volume ratios in very thin films. If the increase in free energy from creating the $PdGa/PdAs_2$ interface is greater than the reduction in free energy realized by transforming to the bulk equilibrium phases, the single

intermediate ternary phase is energetically favorable.

In comparing the data in Table 4.3, there is a general tendency to find binary phases for the thickest Ni films and a single ternary phase for the thinnest ones. But this is not a firm rule. For both the 30 and 74 nm films at 275°C, RBS shows the beginning of In and P segregation and XRD suggests the formation of binary phases. Also Appelbaum and co-workers[85,86] observed a Ni_xIn_yP phase for a 100-nm Ni film annealed at 400°C in an Ar-10%H_2 atmosphere. When a similar sample was annealed instead in He gas at 300°C, laterally separated binary phases were found. Clearly, if there is a thickness effect in the Ni/InP system, it is not the dominant factor.

4.2.3 Annealing Ambient Effect

The effect of the annealing ambient on diffusion in thin films has been studied by Chang and co-workers[87,88,89,90] who have proposed a model based on surface potentials. For a polycrystalline metal (A) film deposited onto a material (B) with less electronegativity, out-diffusion of B through A is enhanced when the annealing ambient creates a negative surface potential change on A. Conversely, B diffusion is supressed for a positive surface potential change on A. This effect is strongest at low temperatures.

The electronegativity differences between Ni and In or P are much smaller those in most systems studied by Chang and co-workers. This may result in a more subtle annealing

ambient effect for the Ni/InP system. Nevertheless, one would expect In (P), which is slightly less (more) electronegative than Ni (In - 1.7, P - 2.1, and Ni - 1.8)[91] to diffuse through the Ni film more (less) readily in an annealing ambient that creates a negative surface potential change on Ni. Conversely, for an annealing ambient that induces a positive surface potential change on Ni, In diffusion will be supressed and P diffusion enhanced.

Adsorption of H_2 gas causes an increase in the Ni work function[92] and, therefore, a positive surface potential change, which should decrease In and increase P diffusion. One would expect this to encourage a reacted phase or phases with P enhancement at the surface and In enhancement near the substrate. No such elemental arrangement has been reported, in spite of the fact that most annealing gases in Table 4.3 contained H_2. Work function data for Ni in Ar, N_2, and He are not available. But rare gases such as Ar are known to decrease the work function of a number of metals.[93] If Ar does induce a negative surface potential change on Ni, and this effect is greater that the opposite effect of the H_2 in these Ar-H_2 gas mixtures, then segregation of In to the surface and P to the substrate would be expected. This is consistent with the results of this study where Ar-5%H_2 was used. Appelbaum, et al. used Ar-10%H_2, and found a single ternary phase rather than In - P segregation. Perhaps the increased H_2 concentration was enough to counteract the

negative surface potential change caused by the Ar. Adsorption of O_2 gas causes a 4 times greater increase in the Ni work function than does H_2. If O_2 were present in the annealing gas, the effect would be the same as for H_2, i.e. increased P and decreased In diffusion. The study by Sands, et al. reported In_2O_3 oxide at Ni_2InP grain boundaries, so some oxygen must have been available during the reaction. If the concentration had been high enough, it could have favored formation of ternary phases rather that a segregated structure.

In a study by Chang and Quintana[94] of Au diffusion through Pt films, they observed that at 350°C the diffusion rate is greatly affected by the annealing ambient. They found that Au outdiffuses 15 times faster in N_2 and 30 times faster in He ambients than in vacuum. They suggested that the gas molecules actually enter the grain boundaries and, thereby, affect the diffusion process. The diameter of the gas molecule may also be an important factor in the increased diffusion rate with the smallest molecules causing the greatest effect.

4.3 Conclusions

In spite of low-temperature, ternary phases with many of the same useful properties that were seen in the Pd/InP system, the reproducibility of the Ni results are unreliable. Subtle changes in the InP native oxide thickness, Ni layer thickness, and annealing ambient gas composition can greatly

influence the outcome of annealing treatments. The results can range from single ternary phases to binary phases arranged in sharply defined layers. This lack of consistency makes Ni difficult, at best, as a component in InP metallizations.

The remainder of this study will focus on Pd as a component for InP metallizations. The next chapter will report preliminary results from a study of a Ge/Pd/InP layered structure.

Chapter 5

5 Ge/Pd/InP METALLIZATION

5.1 Experimental Results

5.1.1 As-Received

The sample was prepared by depositing a 40-nm layer of Pd onto a (100) InP substrate, annealing at 180°C for 30 min, and evaporating a 120-nm Ge layer over this. (Details can be found in Chapter 2.) In making TEM specimens the material was heated to about 95°C for 1 hr in order to cure the epoxy used to bond the cross-section pieces together. A TEM image of this material viewed in cross-section (Fig. 5.1a) shows three distinct layers on the InP. The outermost layer is amorphous Ge (Fig. 5.1b), although in the figure much of this layer has been milled away. In other areas, where the layer was complete, it was found to be approximately 110 nm thick.

The layer adjacent to the substrate is about 35 nm in thickness and forms a smooth interface with InP. The microdiffraction pattern (Fig. 5.1c) shows that this layer is amorphous with interatomic distances of 0.231 and 0.128 nm. These results match well with the amorphous Pd_5InP phase found for Pd/InP after annealing at 175°C (see section 3.1.2).

The Ge and Pd_5InP regions are separated by an intervening polycrystalline layer 15 -20 nm in thickness. Spots seen in microdiffraction match plane spacings expected for PdGe. This result is confirmed by x-ray diffraction as shown in Table

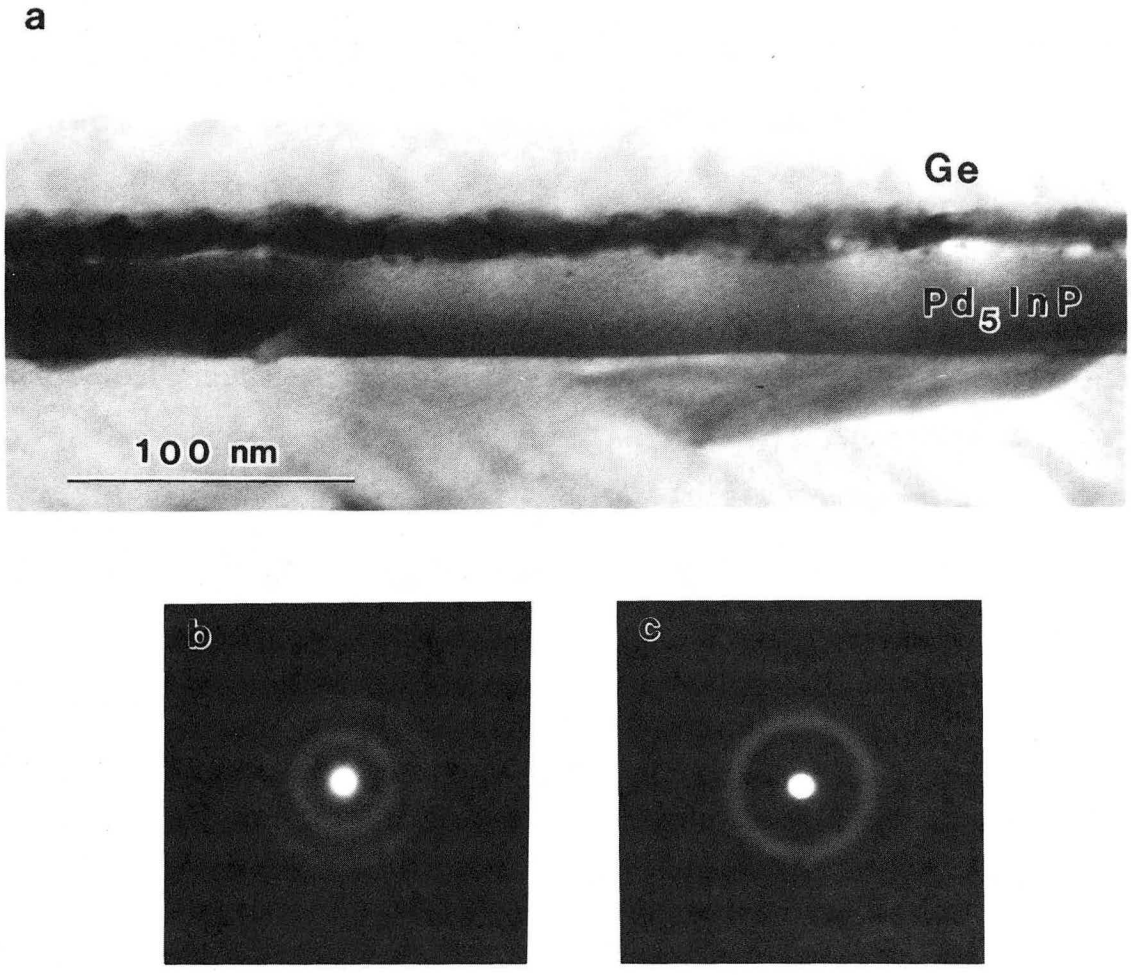

Figure 5.1 Cross-sectional TEM image of Ge/Pd/InP sample as-received is shown in (a). The material underwent a heat treatment at 180°C for 30 min between deposition of the Pd and Ge layers. The microdiffraction pattern in (b) shows that the Ge overlayer is amorphous. The layer adjacent to the InP substrate is identified by (c) as amorphous Pd_5InP.

TABLE 5.1

Ge/Pd/InP As-Received

Pd/InP 180°C 30 min + Ge Overlayer

XRD plane spacings	InP	Ge	PdGe	Pd_2Ge
0.3241 nm		0.3267 nm (111)		
0.2928	0.2934 nm (200)			
0.2627			0.2625 nm (201)	
0.2135			0.2124 (202)	
0.2111			0.2096 (211)	
0.1943			0.1962 (103)	0.1938 nm (300)
0.1916				
0.1464	0.1467 (400)			0.1470 (202)

5.1. An interesting feature of this structure is the very light contrast at the PdGe/Pd_5InP interface. It is unlikely that this feature is an oxide layer since the deposition was done in a vacuum of 10^{-8} torr with no break in vacuum between layers. There may be small voids caused by rapid outdiffusion of Pd from Pd_5InP to the Ge. This was seen by Sands and co-workers[95] for a Si/Ni/GaAs structure prepared in a similar way.

5.1.2 Reaction at 205°C

Samples annealed at 205°C for 4 hr were examined in cross-section in TEM as shown in Figure 5.2. The reacted region between the Ge and InP contains two distinct layers approximately equal in thickness. Between these layers the interface has light contrast and is as thick as 3 nm in some areas. The position of this interface seems to correspond to that of the PdGe/Pd_5InP interface in the as-received sample seen in Figure 5.1.

Selected area diffraction of these layers shows spots that can be indexed as the $[10\bar{1}]$ pole of PdGe (orthorhombic with a = 0.5782, b = 0.3481, and c = 0.6259 nm). This pattern has an epitaxial relation to the InP substrate given by

$$[10\bar{1}]\ \text{PdGe} \parallel [110]\ \text{InP}$$

$$(1\bar{1}1)\ \text{PdGe} \parallel (1\bar{1}1)\ \text{InP}$$

with a -8.2% mismatch for PdGe planes referred to the corresponding InP planes.

In addition to the PdGe reflections, there is an extra

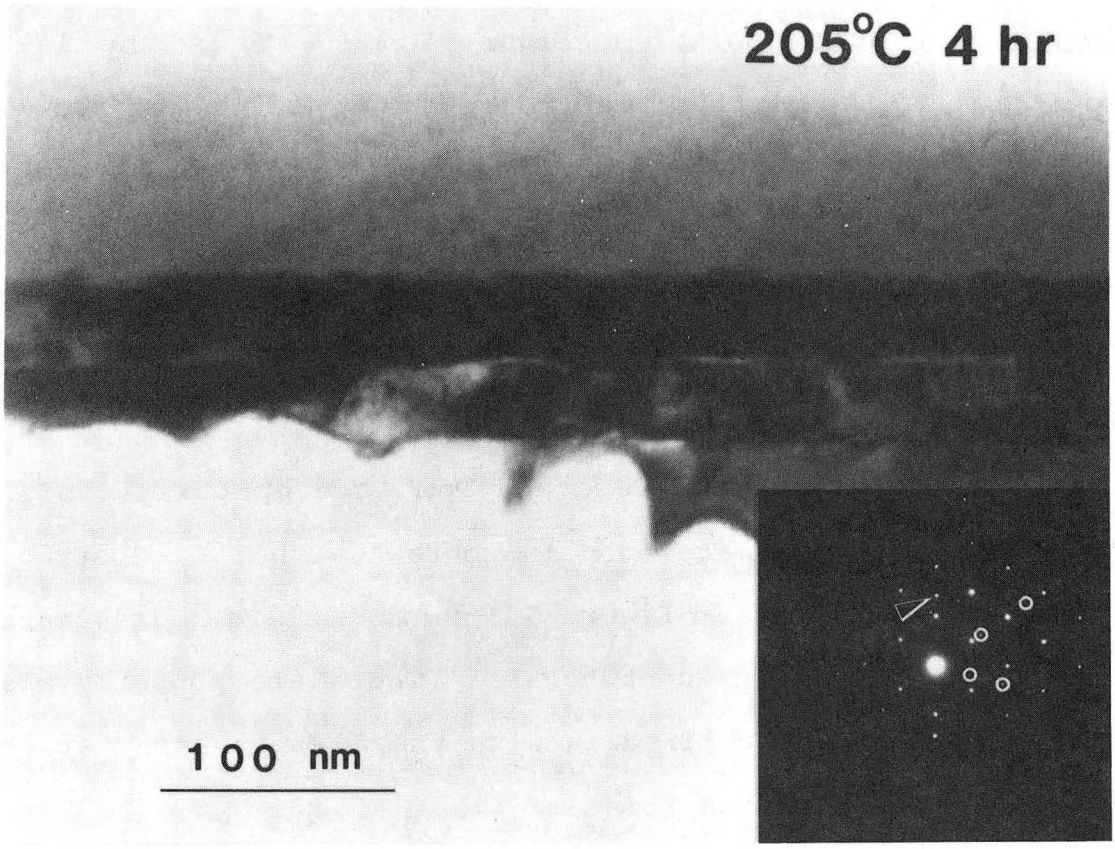

Figure 5.2 Image of Ge/Pd/InP annealed at 205°C for 4 hr viewed in cross section. Selected area diffraction pattern in inset shows InP [110] pattern with epitaxial PdGe reflections indicated by circles. Arrow points to Pd_7P_3 diffraction spot.

spot that lies along the InP [001] direction. This corresponds to a d-spacing of 0.207 nm. This spot was used to form the dark field image shown in Figure 5.3. It is the layer adjacent to the substrate from which this spot comes. Microdiffraction patterns from this region can be indexed as the [211] pole of Pd_7P_3. This same pattern was seen for the Pd/InP system in Figure 3.6 at the amorphous Pd_5InP/InP interface where Pd_7P_3 nuclei had formed after annealing at 175°C.

The fact that both PdGe and Pd_7P_3 are epitaxial to InP indicates that they are both in contact with the substrate. The dark field image in Figure 5.3 shows that Pd_7P_3 is located only in the layer adjacent to InP. There are probably also small grains of PdGe mixed in with the Pd_7P_3 at least at the interface with InP.

5.1.3 Reaction at 325°C

A Ge/Pd/InP sample was annealed at 325°C for 30 min and examined in cross-section in TEM as shown in Fig. 5.4. The layer next to the amorphous Ge contains large grains, many of which seem to have grown through the faint line that corresponds to the original PdGe/Ge interface. The layer next to the InP has a smaller grain structure. Its outer boundary seems to correspond to the original PdGe/Pd_5InP interface in the as-received sample.

Selected area diffraction showed a 0.206-nm spot parallel to InP [002], probably the same as the spot attributed to

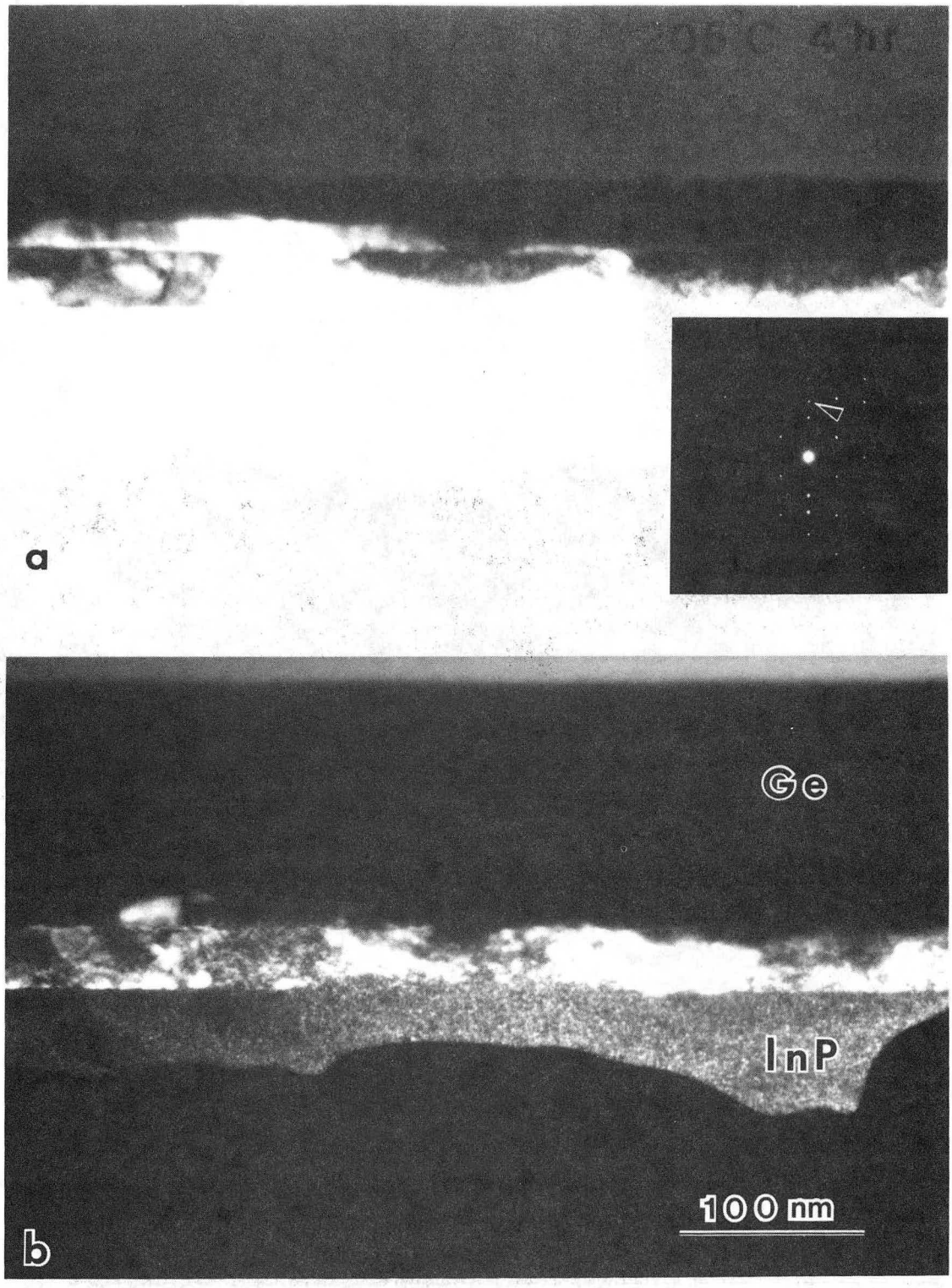

Figure 5.3 Cross-section (a) bright field and (b) dark field images from the same area of a Ge/Pd/InP sample annealed at 205°C for 4 hr. In InP [110] diffraction pattern in inset, arrow points to Pd_7P_3 reflection used in dark field image. This reflection comes from the layer adjacent to the InP substrate.

XBB 890-1590

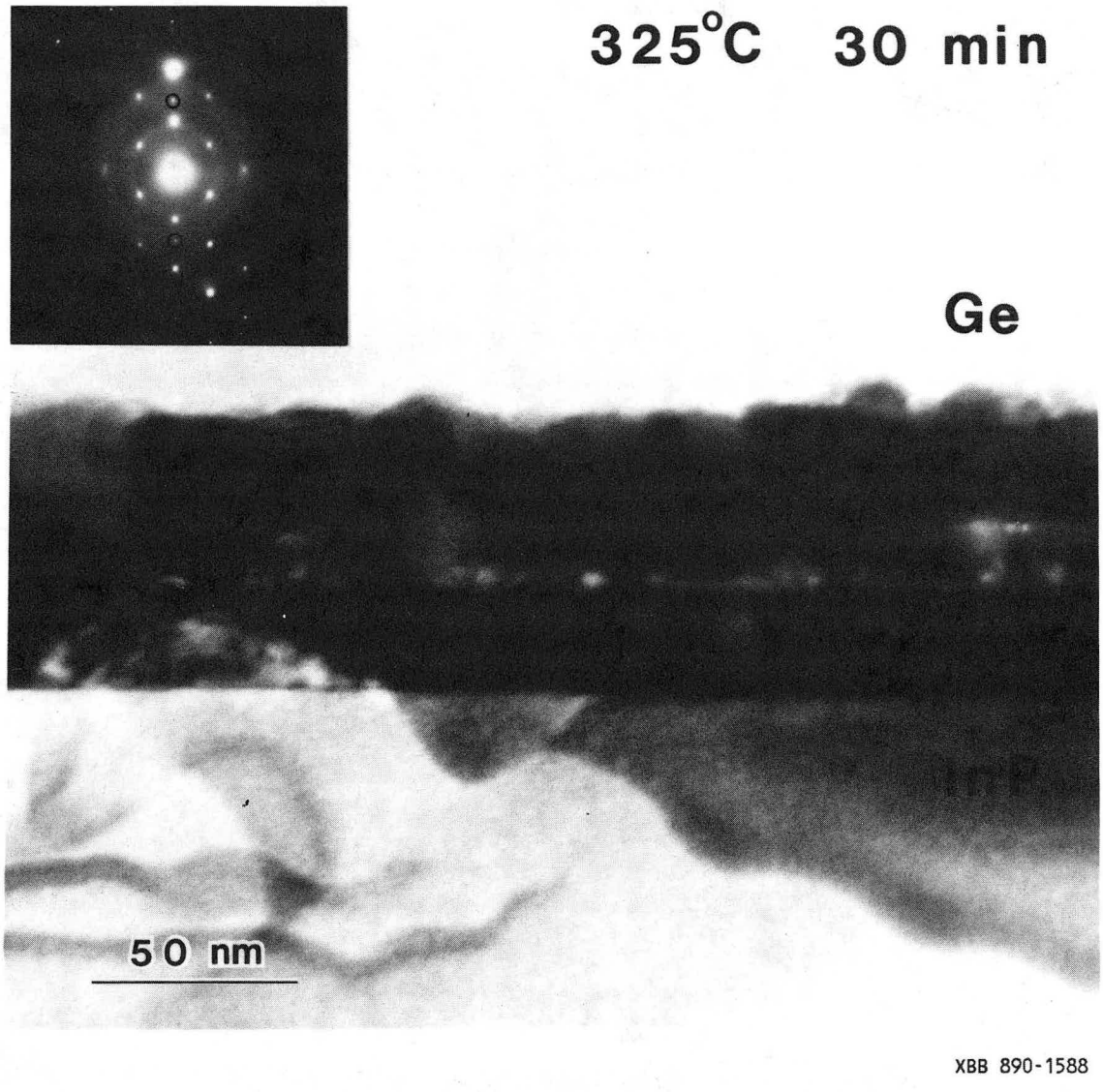

Figure 5.4 Ge/Pd/InP sample annealed at 325°C for 30 min viewed in cross section. Borders of PdGe phase in as-received sample are still visible; the upper one within the newly grown PdGe layer and the lower one at the interface of the PdGe and multiphase layers. InP [110] diffraction pattern in inset shows extra reflections from reacted phase(s) indicated by circles.

Pd_7P_3 for the 205°C sample. Microdiffraction showed evidence of polycrystalline PdGe within the reacted region.

In plan view, this sample exhibited a polycrystalline morphology with some large dark patches due to incomplete removal of one of the layers. The diffraction pattern seen most often has four-fold symmetry with d-spacings of 0.207 and 0.147 nm. Usually two such patterns appear together rotated at various angles one with respect to the other. The patterns in Figure 5.5 have rotation angles of about 54° and 11°, along with very many additional spots that arise from double diffraction. This pattern can also be indexed as Pd_7P_3, but it would not be consistent with the structure of this phase to see the same 0.206 - 0.207 nm plane spacings at right angles to one another in plan view and also in cross section. The hexagonal structure does not have three sets of the same plane that are mutually perpendicular.

The plan-view diffraction pattern shown in Figure 5.6 contains both polycrystalline rings and spots. The diameters of the polycrystalline rings have ratios that indicate a face-centered cubic structure, and their d-spacings agree well with those of Pd. The spots have an epitaxial relation to the InP substrate, with d-spacings of 0.202 and 0.143 nm and index as the Ge [100] pattern. Care was taken to compare this pattern very closely with the patterns in Figure 5.5. Although they are similar, reflections forbidden in Ge appear in the Figure 5.5 patterns and, whereas the difference between 0.206 and

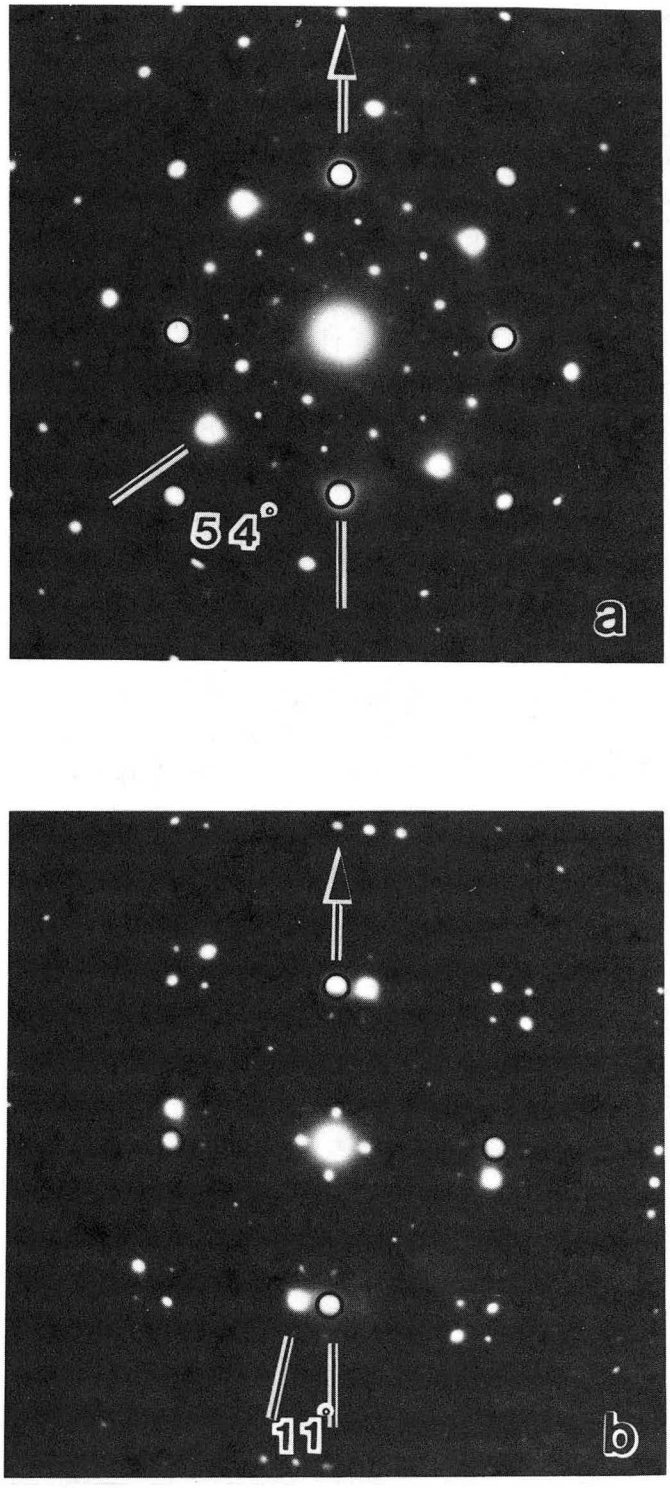

Figure 5.5 Selected area diffraction patterns from plan-view Ge/Pd/InP sample annealed at 325°C for 30 min. Both contain two orientations of a basic pattern, which has 4-fold symmetry, and is indicated by the circles. The second pattern in a) is rotated 54° with respect to the first pattern. The rotation angle in b) is 11°. All additional spots in these patterns are due to double diffraction. The arrows indicate the InP <220> direction.

XBB 893-2656

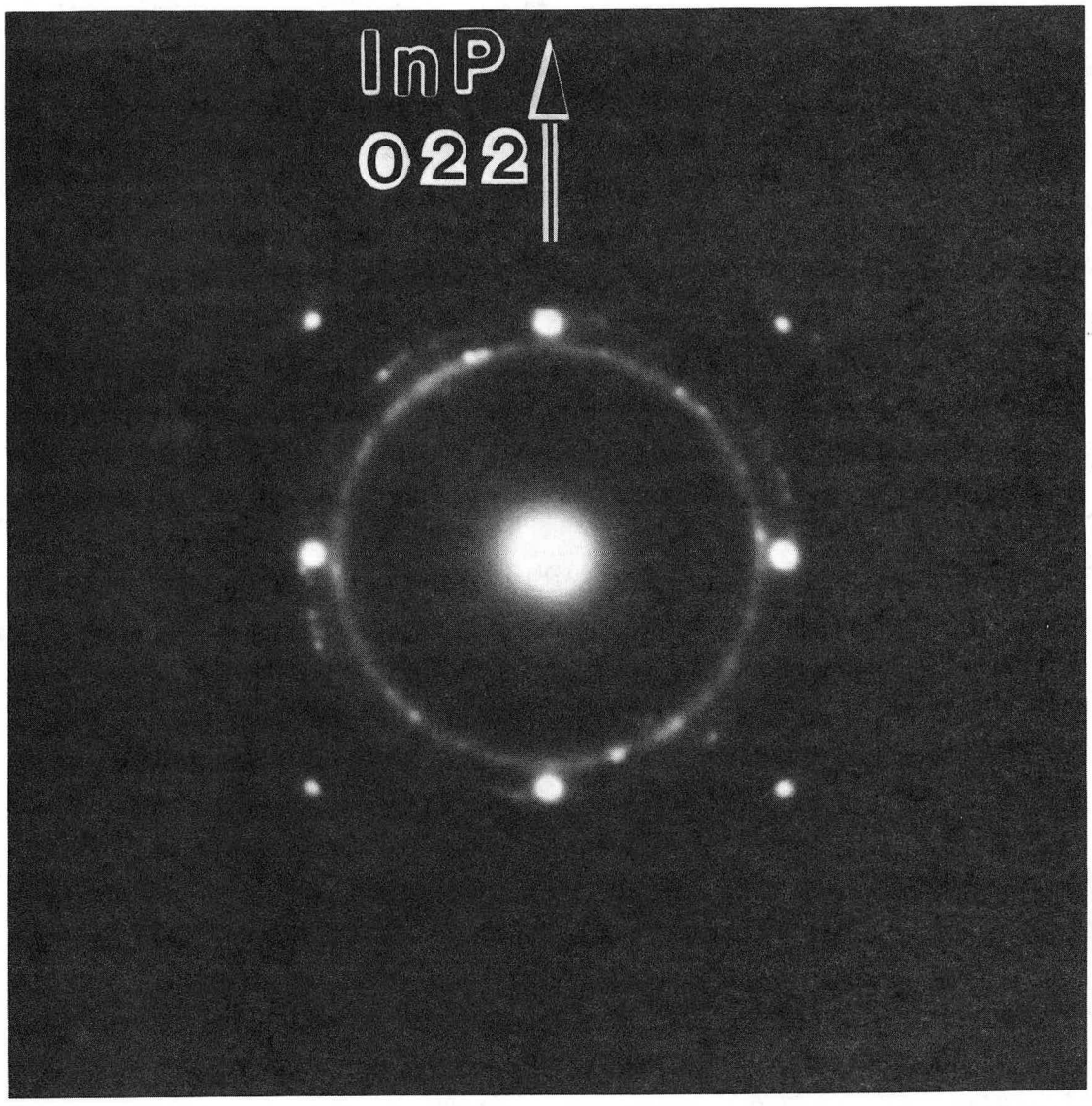

XBB 893-2655

Figure 5.6 Selected area diffraction pattern from plan-view Ge/Pd/InP sample annealed at 325°C for 30 min. Spots are from Ge and polycrystalline rings from Pd. The arrow indicates the InP <220> direction.

0.207 nm may not be significant, the difference between 0.202 and 0.206 nm is. Clearly, the diffraction patterns in Figures 5.5 and 5.6 are not from the same phase.

This same material was annealed an additional 90 min at 325°C, for a total of 120 min at this temperature. The most notable change, as seen in the micrograph in Fig 5.7 is in the thickness and grain size of the layer next to the Ge overlayer. The layer adjacent to the InP is thin enough in some areas to see a grain structure that may be a mixture of phases. Microdiffraction showed large numbers of spots with no apparent order, indicating a mixture of two or more randomly-oriented phases. Some of the strongest spots match d-spacings for PdGe. The original PdGe boundaries are still visible, although they are less prominent.

The XRD results from the 325°C 120 min sample are listed in Table 5.2 Some agreement with Pd_7P_3 can be found, although the very strong peaks at 0.3847 and 0.2043 nm (indicated by underlining) are not from this phase. The 0.2043-nm plane spacing is within experimental error of the 0.206 - 0.207-nm d-spacing of the extra spot along InP [001] seen for samples annealed at 205 and 325°C and may be a more accurate measurement. It is likely that these are from the same planes, but not from the Pd_7P_3 $\{4\bar{4}02\}$ planes, whose d-spacing is 0.2089 nm.

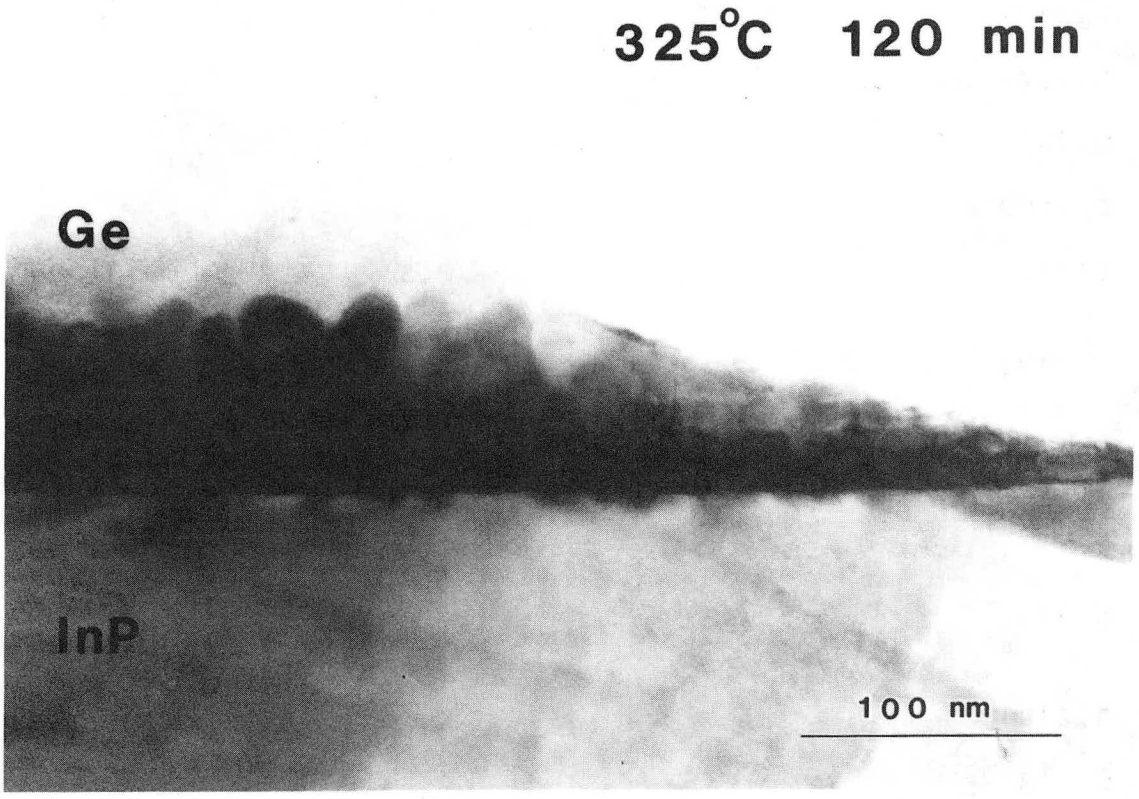

Figure 5.7 TEM image of Ge/Pd/InP cross-section sample annealed at 325°C for 120 min. The original PdGe borders from the as-received sample are still visible, although fainter than before. The PdGe phase next to the Ge overlayer had undergone considerable grain growth. The layer adjacent to the InP substrate may be a mixture of two or more phases.

TABLE 5.2 Ge/Pd/InP 325°C 120 min

XRD plane spacings	InP	Ge	Pd_7P_3	Ge-In phase ?
0.4074 nm				
0.3847				
0.3559				
0.3437			0.3427 nm (211)	
0.3324			0.3340 (012)	
0.3218				
0.3108			0.2994 (220)	
0.2938	0.2934 nm (200)		0.2917 ($02\bar{2}$)	
0.2493				
0.2421			0.2434 (401)	
0.2285			0.2263 (410)	
0.2043		0.2000 nm (220)		
0.1901			0.1889 (241)	
0.1783			0.1788 (502)	
0.1697				
0.1657			0.1657 (431)	
0.1622			0.1631 (143)	
0.1527			0.1522 (333)	
0.1464	0.1467 (400)			

5.2 Discussion

Solid-phase regrowth reactions for fabrication of GaAs contacts have been developed by Sands, Marshall, and Wang[96] and are described in Section 1.3.3. They studied reactions in a layered Si/Ni/GaAs structure and used a buried AlAs marker layer within the GaAs as a fixed reference point from which to measure changes in GaAs at its surface. After annealing at 250°C, they found a Si/Ni-Si/Ni_xGaAs/GaAs structure. Approximately 115 nm of GaAs had been consumed in formation of the Ni_xGaAs ternary phase. Further annealing at 350°C resulted in growth of the Ni-Si layer and regrowth of epitaxial, faulted GaAs by the reaction:

$$xSi + Ni_xGaAs \rightarrow xNiSi + GaAs.$$

Voids were seen in TEM near the top of the regrown GaAs layer as a result of rapid outdiffusion of Ni from Ni_xGaAs to Si during annealing.

A similar structure in the Ge/Pd/GaAs system has been studied by Marshall and co-workers.[97,98] They deposited a layered structure of Ge(125 nm)/Pd(50 nm) onto chemically-cleaned GaAs [100] wafers. The as-deposited sample showed a continuous layer of Pd_xGa_yAs at the Pd/GaAs interface. After annealing at 325°C for 30 min, they found a layered Ge/PdGe/Ge(epitaxial)/InP structure. They reasoned that the initial Pd - GaAs reaction may have created an excess of Ga vacancies in the GaAs. An n^+ GaAs layer was formed as the Ge diffused into the substrate and filled these vacancies.

Because of the large amount of excess Ge, solid-phase transport through the PdGe layer and epitaxial growth of Ge onto the GaAs occured. They concluded that conditions for ohmic contact formation in this system include initial contact between Pd and the GaAs substrate and an amount of Ge in excess of that needed for PdGe formation. Another interpretation, in light of the Si/Ni/GaAs results discussed above, is that a very thin n^+ GaAs layer may have regrown onto the substrate during decomposition of the Pd_xGa_yAs phase.

A diagram summarizing the results of the present study with preliminary phase identification is shown in Figure 5.8. The surface of the Ge layer is used as a frame of reference from which to compare the layer thickness for different heat treatments. This can be only a rough guide and may not be in a fixed position relative to the unreacted InP since the thicknesses of the reacted layers change depending on their densities. Notice that voids at the boundaries of the PdGe layer in the as-received sample seem to persist throughout the annealing. Their constant position argues in support of the Ge surface as a frame of reference.

In the present study, the annealing of Pd/InP in vacuum before deposition of the Ge overlayer results in formation of the amorphous ternary Pd_5InP phase as expected from the results in Chapter 3. After Ge deposition, a thin layer of PdGe forms at the Ge/Pd_5InP interface, which increases in thickness and grain size as the annealing time and temperature

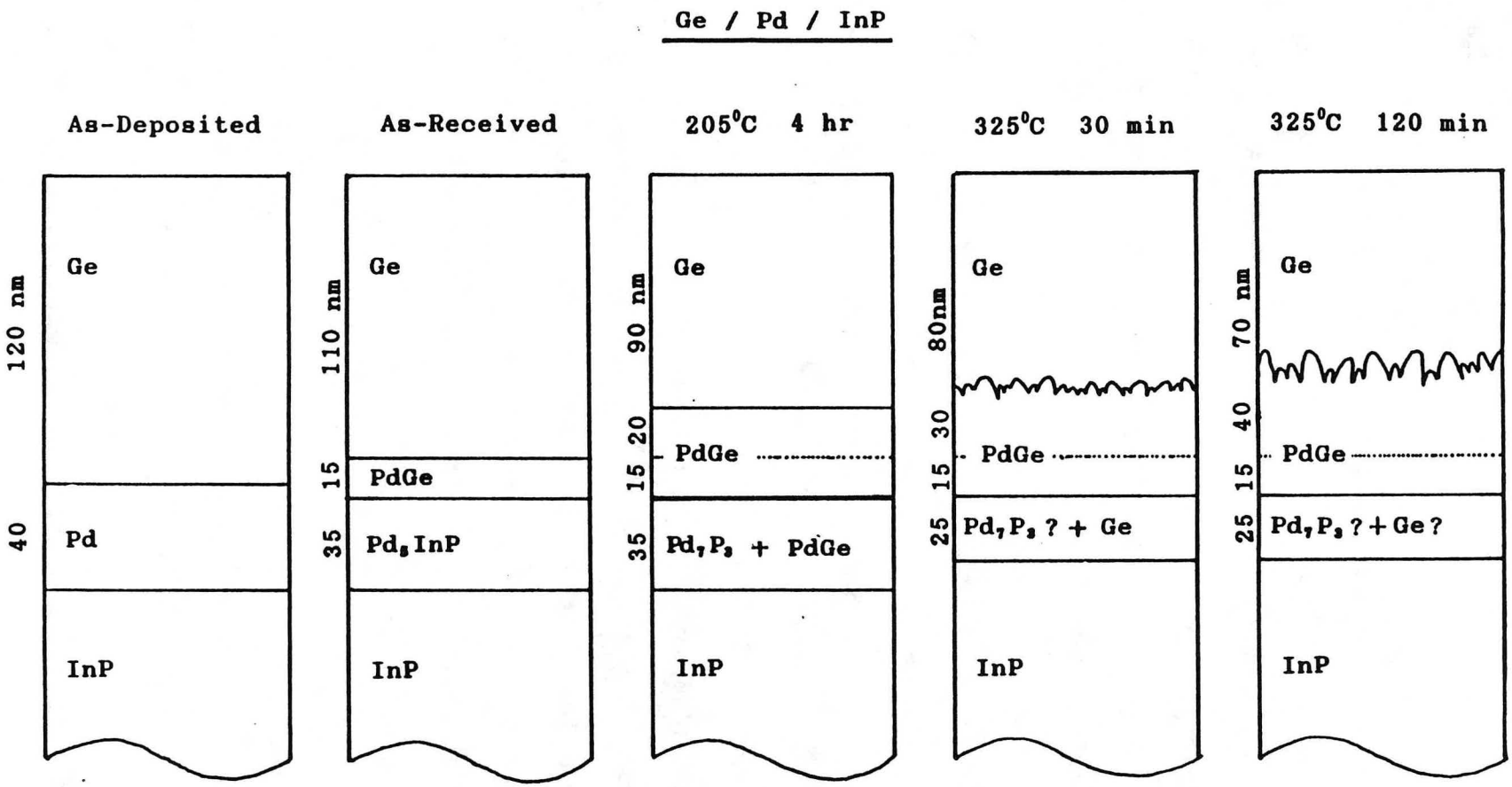

Figure 5.8 Schematic drawing summarizing TEM results for Ge/Pd/InP sample with layer thicknesses indicated. Note that voids positioned at the original PdGe interfaces in the as-received sample seem to persist after annealing.

are increased. A PdGe layer was also observed in the Ge/Pd/GaAs study.

Identification of the layer next to the InP is not as straightforward in this system as it was for the GaAs metallizations. The Pd_5InP phase decomposes after annealing at 205°C, and the Pd_7P_3 phase appears in the layer next to the InP substrate. For the Pd/InP system, as shown in Figure 3.6, nuclei of the Pd_7P_3 phase formed at the amorphous Pd_5InP/InP interface after annealing at 175°C, but this phase was not seen again at higher temperatures. There may be a very fine free energy balance between crystallization of Pd_5InP and formation of Pd_7P_3. It is interesting to note that Pd_5InP is slightly richer in Pd than Pd_7P_3. If Pd_7P_3 were favored in an environment of reduced Pd, then formation of this phase could be explained for Ge/Pd/InP. Much of the Pd in the amorphous Pd_5InP diffuses away toward the surface to react with Ge, thus causing growth of the PdGe layer. At this temperature, Ge diffuses in toward the substrate, as evidenced by PdGe diffraction spots epitaxial to InP. The fate of the In species is unclear.

After annealing at 325°C, the position of the InP interface suggests that there may have been some regrowth of the InP substrate, although no evidence of faulting or interface irregularity can be seen in Figures 5.4 and 5.7. This may not be surprising at these magnifications. There are some areas of the 325°C specimens that show evidence of Ge

epitaxial to InP, but this is not continuous along the interface. At the present time, the other phases in contact with InP elude identification. In light of excess In that could not be accounted for, it would be reasonable to consider Ge-In phases, but no such phases have been reported.[99]

5.3 Conclusions

The Ge/Pd metallization may be a useful contact for InP. The reacted layer adjacent to the InP forms a smooth layer with no protrusions into the semiconductor. Regrowth of InP and epitaxial growth of a Ge layer adjacent to this, thought to be requirements for good ohmic behavior, may be occuring in this system. Further study is needed to resolve these issues.

6 CONCLUSIONS

As a component in InP metallizations, palladium is a better candidate than nickel because of its insensitivity to the InP native oxide and its aggressiveness in reacting even at room temperature. Formation of a ternary phase at low temperatures is another attractive feature, since both In and P are consumed in equal abundance, thus maintaining the electrical properties of the substrate. Nickel, on the other hand, shows much variety in its reaction products for seemingly identical heat treatment conditions. Its sensitivity to subtle changes in the InP native oxide thickness, Ni layer thickness, and annealing ambient gas make it unreliable as a component in InP contacts.

The Ge/Pd metallization on InP shows promise metallurgically. The PdGe layer formed just below the Ge is well behaved at moderate temperatures, impinging only on the Ge as it grows. The reacted layer adjacent to InP forms a smooth interface with no protrusions into the InP layer. Although some Ge grew epitaxially onto the InP substrate, it was not a continuous, uniform layer, and the question of regrowth of InP is not resolved. Further study will be needed to determine whether conditions necessary for good ohmic contacts can be achieved with this system.

Whereas there has been much study of phase stability and morphology for metal/semiconductor reactions with Si and GaAs

materials, this is one of the first such studies of the more difficult metal/InP systems. Many more will follow.

7 SUMMARY

The main findings of this study are:

1. The reaction between Pd and InP begins at room temperature and is insensitive to the InP native oxide.

2. The first phase formed in the Pd/InP system is an amorphous ternary phase of approximate composition Pd_5InP. This forms a flat interface with InP and is still the dominant phase after annealing at 175°C for 30 min.

3. For capped samples at 450 to 650°C, the only phase found was PdIn. Phosphorus is so volatile at these temperatures that it is difficult to maintain a closed system.

4. The reaction between Ni and InP can also begin at room temperature. Subtle changes in the InP native oxide thickness, Ni layer thickness, and annealing ambient gas composition make reproducibility of these results unreliable.

5. The first Ni/InP reaction product is an amorphous ternary phase.

6. Under certain conditions, Ni/InP reaction products at higher temperatures are layered structures in the sequence In-Ni phase/Ni_2P/InP.

7. The Ge/Pd_5InP(amorphous)/InP layered structure maintains a smooth interface at InP for annealing at temperatures up to 325°C.

8. The layer adjacent to InP comprises a mix of epitaxial phases, one of which is Ge.

9. Growth of the PdGe phase next to the Ge results in a very irregular interface with Ge while maintaining a smooth interface with the layer adjacent to the InP.

8 REFERENCES

1. T.S. Kuan, J.L. Freeouf, P.E. Batson, and E.L. Wilkie, **J. Appl. Phys. 58,** 1519 (1985).

2. T. Sands, V.G. Keramidas, R. Gronsky, and J. Washburn, **Thin Solid Films, 136,** 105 (1986).

3. T. Sands, V.G. Keramidas, J. Washburn, and R. Gronsky, **Appl. Phys. Lett. 48,** 402 (1986).

4. W. Schottky, **Naturwissenschaften 26,** 843 (1938).

5. J. Bardeen, **Phys. Rev. 71,** 717 (1947).

6. W.E. Spicer, P.W. Chye, P.R. Skeath, C.Y. Su, and I. Lindau, **J. Vac. Sci. Technol. 16,** 1422 (1979).

7. W.E. Spicer, I. Lindau, P. Skeath, and C.Y. Su, **J. Vac. Sci. Technol. 17,** 1019 (1980).

8. W.E. Spicer, I. Lindau, P. Skeath, C.Y. Su, and P. Chye, **Phys. Rev. Lett. 44,** 420 (1980).

9. J.L. Freeouf and J.M Woodall, **Appl. Phys. Lett. 39,** 727 (1981).

10. J. M. Woodall and J.L. Freeouf, **J. Vac. Sci. Technol. B 2,** 510 (1984).

11. V. Heine, **Phys. Rev. A 138,** 1689 (1965).

12. J. Tersoff, **Phys. Rev. Lett. 52,** 465 (1984).

13. G. Hughes, R. Ludeke, F. Schaffler, and D. Rieger, **J. Vac. Sci. Technol. B 4,** 924 (1986).

14. O.F. Sandkey, R.E. Allen, S-F. Ren, and J.D. Dow, **J. Vac. Sci. Technol. B 3,** 1162 (1985).

15. K.J. Schulz, X.-Y. Zheng, and Y.A. Chang, **Electronic Packaging Materials Science,** Eds. R. Jaccodine, K.A. Jackson, and R.C. Sundahl. (Mater. Res. Soc., Pittsburgh, 1988) p. 455.

16. A. Lahav, M. Eizenberg and Y. Komem, **J. Appl. Phys. 62,** 1768 (1987).

17. K. Suh, H.K. Park, and K.L. Moazed, **J. Vac. Sci. Technol. B1,** 365 (1983).

18. K.M. Yu, S.K. Cheung, T. Sands, J.M. Jaklevic, N.W. Cheung, and E.E. Haller, **J. Appl. Phys. 60,** 3235 (1986).

19. T. Sands, V.G. Keramidas, A.J. Yu, R. Gronsky, and J. Washburn, **J. Mater. Res. 2,** 262 (1987).

20. T.S. Kuan, J.L. Freeouf, P.E. Batson, and E.L. Wilkie, **J. Appl. Phys. 58,** 1519 (1985).

21. T. Sands, V.G. Keramidas, R. Gronsky, and J. Washburn, **Thin Solid Films 136,** 105 (1986).

22. M. Ogawa, **Thin Solid Films 70,** 181 (1980).

23. A Lahav and M. Eizenberg, **Appl. Phys. Lett. 45,** 256 (1984).

24. T. Sands, V.G. Keramidas, J. Washburn, and R. Gronsky, **Appl. Phys. Lett. 48,** 402 (1986).

25. T. Sands, V.G. Keramidas, A.J. Yu, R. Gronsky, and J. Washburn, **J. Mater. Res. 2,** 262 (1987).

26. T. Sands, V.G. Keramidas, A.J. Yu, K.M. Yu, R. Gronsky, and J. Washburn, **J. Mater. Res. 2,** 262 (1987).

27. N. Braslau, J.B. Gunn, and J.L. Staples, **Solid-State Electron. 10,** 372 (1967).

28. A. Christou, **Solid-State Electron. 22,** 141 (1979).

29. N. Braslau, **J. Vac. Sci. Technol. 19,** 803 (1981).

30. T.S. Kuan, P.E. Batson, T.N. Jackson, H. Rupprecht, and E.L. Wilkie, **J. Appl. Phys. 54,** 6952 (1983).

31. T. Sands, **Materials Science & Engineering B1,** 289 (1989).

32. C.J. Palmstrom and D.V. Morgan in **Gallium Arsenide** edited by M.J. Howes and D.V. Morgan (Wiley, Chichester, 1985) Chap. 2.

33. G.Y. Robinson, in **Physics and Chemistry of III-V Compound Semiconductor Interfaces** edited by C.W. Wilmsen (Plenum, New York, 1985) Chap. 2.

34. E. Hokelek and G.Y. Robinson, **Appl. Phys. Lett. 40,** 426 (1982).

35. L.J. Brillson, C.F. Brucker, A.D. Katnani, N.G. Stoffel, R. Daniels, and G. Margaritondo, **J. Vac. Sci. Technol. 21,** 564 (1982).

36. T. Kendelewicz, N. Newman, R.S. List, I. Lindau, and W.E. Spicer, **J. Vac. Sci. Technol. B3,** 1206 (1985).

37. T. Sands, E.D. Marshall, and L.C. Wang, **J. Mater. Res. 3,** 914 (1988).

38. E.D. Marshall, W.X. Chen, C.S. Wu, S.S, Lau, and T.F. Kuech, **Appl. Phys. Lett. 47,** 298 (1985).

39. L.C. Wang, B. Zhang, F. Fang, E.D. Marshall, S.S. Lau, T. Sands, and T.F. Kuech, **J. Mater. Res. 3,** 922 (1988).

40. T. Sands, E.D. Marshall, and L.C. Wang, **J. Mater. Res. 3,** 914 (1988).

41. G. Cliff and G.W. Lorimer, **J. Micros. 103,** 203, (1975).

42. M. El-Boragy and K. Schubert, **Z. Metallkde. 61,** 579 (1970).

43. R.B. Schwarz and W.L. Johnson, **Phys. Rev. Lett. 51,** 415 (1983).

44. R.B. Schwarz, K.L. Wong, and W.L. Johnson, **J. Non-Cryst. Solids 61/62,** 129 (1984).

45. B.M. Clemens, R.B. Schwarz, and W.L. Johnson, **J. Non-Cryst. Solids 61/62,** 817 (1984).

46. M. Atzmon, J.D. Verhowven, E.D. Gibson, and W.L. Johnson, **Appl. Phys. Lett. 45,** 1052 (1984).

47. M. van Rossum, M.-A. Nicolet, and W.L. Johnson, **Phys. Rev. B 29,** 5498 (1984).

48. H. Schroder, K. Samwer, and U. Koster, **Phys. Rev. Lett. 54,** 197 (1985).

49. P. Guillmin, P. Guyot, and G. Marchal, **Phys. Lett. 109A,** 174 (1985).

50. B.M. Clemens and M.J. Suchoski, **Appl. Phys. Lett. 47,** 943 (1985).

51. B.M. Clemens, **Phys. Rev. B 33,** 7615 (1986).

52. H. Schroder, K. Samwer, and U. Koster, **Phys. Rev. Lett. 54,** 197 (1985).

53. W.L. Johnson, **Progress in Material Science 30,** 81 (1986).

54. X.L. Yeh, K. Samwer, and W.L. Johnson, **Appl. Phys. Lett. 42,** 242 (1983).

55. X.L. Yeh and E.J. Cotts, **J. Mater. Res. 2,** 173 (1987).

56. X.L. Yeh, K. Samwer, and W.L. Johnson, **Appl. Phys. Lett. 42,** 242 (1983).

57. R.M. Walser and R.W. Bene, **Appl. Phys. Lett. 28,** 624 (1976).

58. R.P. Elliot, **Constitution of Binary Alloys,** First Supplement (McGraw-Hill, New York, 1965) p. 549.

59. M. Hansen and K. Anderko, **Constitution of Binary Alloys,** 2nd Edition (McGraw-Hill, New York, 1958) p. 1084.

60. M. El-Boragy and K. Schubert, **Z. Metallkde. 61,** 579 (1970).

61. T. Sands, C.C. Chang, A.S. Kaplan, V.G. Keramidas, K.M. Krishnan, and J. Washburn, **Appl. Phys. Lett. 50,** 1346 (1987).

62. T.S. Kuan, J.L. Freeouf, P.E. Batson, and E.L. Wilkie, **J. Appl. Phys. 58,** 1519 (1985).

63. T. Sands, V.G. Keramidas, R. Gronsky, and J. Washburn, **Thin Solid Films 136,** 105 (1986).

64. T. Sands, V.G. Keramidas, R. Gronsky and J. Washburn, **Thin Solid Films 136,** 105 (1986).

65. R.F.C. Farrow, **J. Phys. D: Appl. Phys. 7,** 2436 (1974).

66. J.D. Oberstar, B.G. Streetman, and E.A. Sammann, **Thin Solid Films 81,** 347 (1981).

67. J.P. Donnelly and C.E. Hurwitz, **Appl. Phys. Lett. 31,** 418 (1977).

68. J.D. Oberstar, B.G. Streetman, J.E. Baker, N.L. Finnegan, E.A. Sammann, and P. Williams, **Thin Solid Films 94,** 149 (1982).

69. C.W. Wilmsen, **Thin Solid Films 39,** 105 (1976).

70. C.W. Wilmsen and R.W. Kee, **J. Vac. Sci. Technol. 15,** 1513 (1978).

71. J.F. Wager and C.W. Wilmsen, **J. Appl. Phys. 51,** 812 (1980).

72. C.W. Wilmsen, **J. Vac. Sci. Technol. 19,** 288 (1981).

73. Art Nelson, Kent Geib, and C.W. Wilmsen, **J. Appl. Phys. 54,** 4134 (1983).

74. T. Sands, C.C. Chang, A.S. Kaplan, V.G. Keramidas, K.M. Krishnan, and J. Washburn, **Appl. Phys. Lett. 50,** 1346 (1987).

75. A. Appelbaum, L.C. Feldman, L.A. Koszi, P.M. Thomas, P.A. Barnes, unpublished.

76. A. Appelbaum, P.M. Thomas, and P.A. Barnes, in **Proceedings of the MRS/TMS Northeast Regional Meeting on Semiconductor-Based Heterostructures-Interfacial Structure and Stability,** edited by M.L. Green, E.E. Baglin, G.Y, Chin, H.W. Deckman, W. Mayo, and K. Narasinham (TMS, Warrendale, PA, 1986), p. 409.

77. T. Sands, C.C. Chang, A.S. Kaplan, V.G. Keramidas, K.M. Krishnan, and J. Washburn, **Appl. Phys. Lett. 50,** 1346 (1987).

78. A. Appelbaum, L.C. Feldman, L.A. Koszi, P.M. Thomas, P.A. Barnes, unpublished.

79. A. Appelbaum, P.M. Thomas, and P.A. Barnes, in **Proceedings of the MRS/TMS Northeast Regional Meeting on Semiconductor-Based Heterostructures-Interfacial Structure and Stability,** edited by M.L. Green, E.E. Baglin, G.Y, Chin, H.W. Deckman, W. Mayo, and K. Narasinham (TMS, Warrendale, PA, 1986), p. 409.

80. T. Sands, C.C. Chang, A.S. Kaplan, V.G. Keramidas, K.M. Krishnan, and J. Washburn, **Appl. Phys. Lett. 50,** 1346 (1987).

81. G.P. Schwartz, W.A. Sunder, and J.E. Griffiths, **J. Electrochen. Soc.: Solid-State Science and Technology 129,** 1361 (1982).

82. Art Nelson, Kent Geib, and C.W. Wilmsen, **J. Appl. Phys. 54,** 4134 (1983) and references therein.

83. S. Singh, R.S. Williams, L.G. Van Uitert, A. Schlierr, I. Camlibel, and W.A. Bonner, **J. Electrochem. Soc.: Solid-State Science and Technology 129,** 447 (1982).

84. T. Sands, V.G. Keramidas, K.M. Yu, J. Washburn, and K. Krishnan, **J. Appl. Phys. 62,** 2070 (1987).

85. A. Appelbaum, L.C. Feldman, L.A. Koszi, P.M. Thomas, P.A. Barnes, unpublished.

86. A. Appelbaum, P.M. Thomas, and P.A. Barnes, in **Proceedings of the MRS/TMS Northeast Regional Meeting on Semiconductor-Based Heterostructures-Interfacial Structure and Stability,** edited by M.L. Green, E.E. Baglin, G.Y, Chin, H.W. Deckman, W. Mayo, and K. Narasinham (TMS, Warrendale, PA, 1986), p. 409.

87. Chin-An Chang, **J. Electrochem. Soc. 127,** 1331 (1980).

88. C.-A. Chang and W.-K. Chu, **Appl. Phys. Lett. 37,** 161 (1980).

89. C.-A. Chang and N.J. Chou, **J. Vac. Sci. Technol. 17,** 1358 (1980).

90. C.-A. Chang, **Appl. Phys. Lett. 38,** 860 (1981).

91. L. Pauling, **The Nature of the Chemical Bond,** 3rd ed., Cornell University Press, New York (1960).

92. G.A. Somorjai, **Principles of Surface Chemistry,** (Prentice-Hall, New Jersey, 1972) p.249.

93. G.A. Somorjai, **Principles of Surface Chemistry,** (Prentice-Hall, New Jersey, 1972) p.249.

94. C.C. Chang and G. Quintana, **Appl. Phys. Lett. 29,** 453 (1976).

95. T. Sands, E.D. Marshall, and L.C. Wang, **J. Mater. Res. 3,** 914 (1988).

96. T. Sands, E.D. Marshall, and L.C. Wang, **J. Mater. Res. 3,** 914 (1988).

97. E.D. Marshall, W.X. Chen, C.S. Wu, S.S. Lau, and T.F. Kuech, **Appl. Phys. Lett. 47,** 298 (1985).

98. E.D Marshall, B. Zhang, L.C. Wang, P.F. Jiao, W.X. Chen, T. Sawada, S.S. Lau, K.L. Kavanagh, and T.F. Kuech, **J. Appl. Phys. 62,** 942 (1987).

99. P. Villars and L.D. Calvert, **Pearson's Handbook of Crystallographic Data for Intermetallic Phases, Vols. 1-3,** (ASM, Metals Park, Ohio) 1985.

LAWRENCE BERKELEY LABORATORY
CENTER FOR ADVANCED MATERIALS
1 CYCLOTRON ROAD
BERKELEY, CALIFORNIA 94720